Effect of Panel Inertia and Stiffness on Rivet Formation Rate during Percussive Riveting

Ryan Daniel Mott

A thesis

submitted in partial fulfillment of the

requirements for the degree of

Master of Science in Mechanical Engineering

University of Washington

2018

Committee:

Per Reinhall

Joseph Garbini

Riley HansonSmith

Program Authorized to Offer Degree:

Mechanical Engineering

University of Washington

Abstract

Effect of Panel Inertia and Stiffness on Rivet Formation Rate during Percussive Riveting

Ryan Daniel Mott

Chairs of the Supervisory Committee:

Per Reinhall
Mechanical Engineering
Joseph Garbini
Mechanical Engineering

Experiments with percussive riveting tools install rivets in surrogate coupons. The validity of the results of these experiments relies on the experiments' similarity to production. This experiment evaluates the variability of the installation process caused by the dynamic characteristics of the coupon. Rivets were installed in specially machined coupons to evaluate how rivet formation rate and the coupon's absorption of momentum depend on the coupon's thickness and on the rivets' distance from a free or supported edge of the coupon. Thicker coupons were found to reduce the momentum transferred from the rivet to the bucking bar and to reduce the rate of rivet formation.

Table of Contents

List of Figures

List of Tables

Dedication

For Rachel

1 Introduction

1.1 Context

1.1.1 Ergonomics of percussive riveting

The assembly of a single aircraft consumes hundreds of thousands of rivets. While automated installation has become common, assembly relies heavily on manual rivet installation using percussive hand tools [1][2]. The thousands of pounds required to compress a rivet are applied by a handheld pneumatic hammer or rivet gun to the head of the rivet, flattening the tail of the rivet against a bucking bar acting as an anvil on the other side of the panels being joined. The powerful impulsive vibration of both the rivet gun and the bucking bar damages mechanics' joints and blood vessels. Common injuries include vibration-induced white finger and carpal tunnel syndrome [1][2][3]. For example, one study of 340 aircraft mechanics found that more than 50% of those with ten or more years installing rivets developed symptoms of vibration-induced white finger [4].

These hazards have prompted the creation of new tool designs which reduce the hazardous vibration of percussive riveting, but the effectiveness of these tools is not always well tested [1] [2]. The Boeing Advanced Research Center (BARC) at the University of Washington tests such tools installing rivets in a laboratory setting to measure both their performance reducing vibration while installing quality rivets.

As with any experiment, the implicit assumption while conducting these tests is that the tools' behavior in the laboratory is analogous their behavior in mechanics' hands on the factory floor. This assumption allows the experimenters to state that a tool which performs better in test will also be superior in production.

1.1.2 The coupon

As with most riveting experiments, the workpiece (an aircraft panel) is replaced by a small surrogate coupon for riveting tests: a rectangular, single-ply sheet typically of the same material, coating, and holes as the workpiece, such as shown in Figure 1.1.

Figure 1.1: Example of surrogate coupon used in riveting tests to evaluate tool effectiveness.

This substitution is valid provided it does not change the riveting process. However, these coupons appear to have substantially influenced the performance of the tools. Tests with 5/16” diameter rivets at the BARC in 2017 were frustrated by a pattern depicted in Figure 1.2, which is most likely attributable to the coupon.

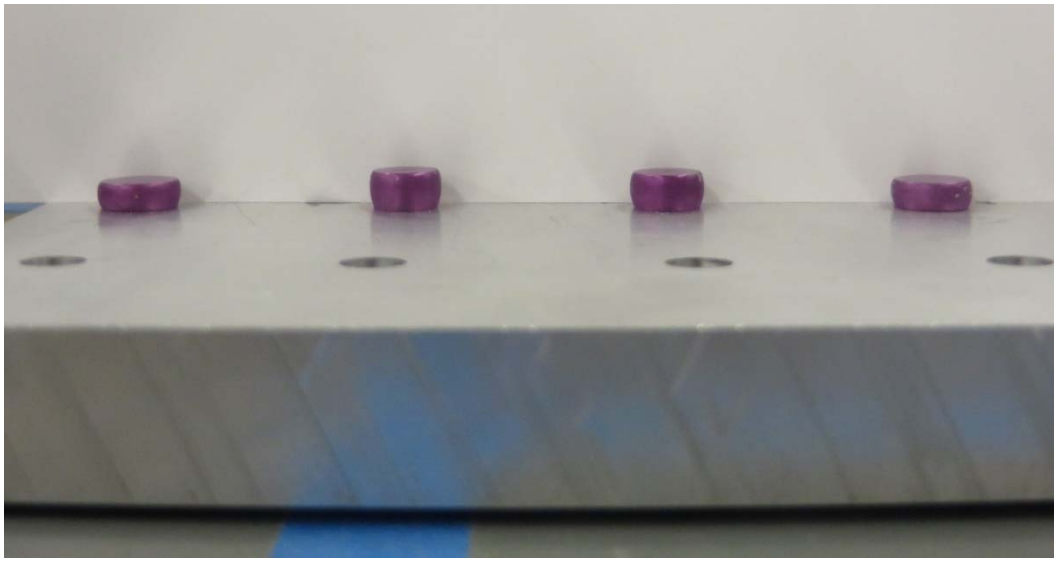

Figure 1.2: 5/16" diameter rivets exhibit dramatic variation in formation rate by position

These coupons had four rows of holes: two nearest the long edges of the coupon, and two nearer to the middle of the coupon. Rivets in the two rows of holes near the edge of the coupon would quickly deform to the desired height during installation, but rivets in the middle two rows would consistently deform less under the same conditions. This pattern suggests that variation in the test coupon – in this case, variation in the distance of the rivet from the edge of the coupon – can dramatically influence the riveting process, specifically the rate of rivet formation.

This variation in the outcome of the riveting process raises questions regarding the validity of riveting tests. If the coupon's influence in the riveting process is so large, is riveting on such a coupon representative of rivet installations in production? Could the difference between the coupon and an aircraft make conclusions in the laboratory invalid in the factory?

1.2 Thesis objective

The issue of the correlation between a coupon and an aircraft requires two steps to answer. One step is to understand how the panels to be joined influence the process of installing

rivets in them. The other is to assess whether the qualities of the coupon which differ from the workpiece are factors in the panels' influence. The objective of the experiment reported here is to explore the former question, that of how variation in the qualities of the coupon affects rivet formation.

The bucking bar's reaction force against the rivet is responsible for deforming the rivet. The duration and magnitude of this force is limited by the momentum transferred from the gun piston through the rivet to the bucking bar. But because the rivet's velocity is limited to the velocity of the coupon, the total momentum from the gun's piston is split between the momentum transferred to the bucking bar and the momentum absorbed by the coupon. Therefore, we can hypothesize that a coupon which absorbs more momentum will reduce the force applied to the rivet, reducing the rate at which the rivet forms. The experiment described in this thesis tests whether increasing the thickness of the coupon or the position of the rivet affects the momentum transferred to the bucking bar and in turn influence the rivet's formation rate.

1.3 Prior work

Ahn describes the design and use of the automated test bench used in this experiment, which is discussed briefly in section 4.1. He used this bench to compare the Ingersoll-Rand AVC27 with the Atlas Copco RRH-12P [1] installing interference-fit bolts. Cherng et al. similarly used a test fixture for controlling experiments to evaluate ergonomically modified tools. The test fixture's coupon is a light, narrow strip [3]. McDowell et. al. proposed a method for evaluating bucking bars which replaces the rivet with a vibration-absorbing structure. All three studies evaluated vibration levels by measuring or estimating the acceleration of the tools.

It is difficult to find existing studies of any aspect of percussive riveting which study the panel's effects on installation. Quasi-static models of the deformation of the rivet are more common than dynamic models [5]. In [5] Xi et. al. study the how a rivet gun mounted on robotic arm can cause the arm to resonate at certain poses. Their model includes the internal components of the rivet gun and divides the rivet into a string of elements, while treating the bucking bar as immoveable and ignoring the panel. One study which incidentally speaks to the motion of the panel investigates reducing noise by reducing the acceleration of the panel. Supporting the panel around the rivet and increasing the mass of the bucking bar both reduced the panel's motion [6].

2 Theoretical foundations

2.1 Mechanics of percussive riveting

Let us dissect the riveting process to establish a defined context for the analysis of percussive riveting, before searching it for the panel's means of influencing the process. The state of the system immediately before the rivet gun's first strike is depicted in Figure 2.1.

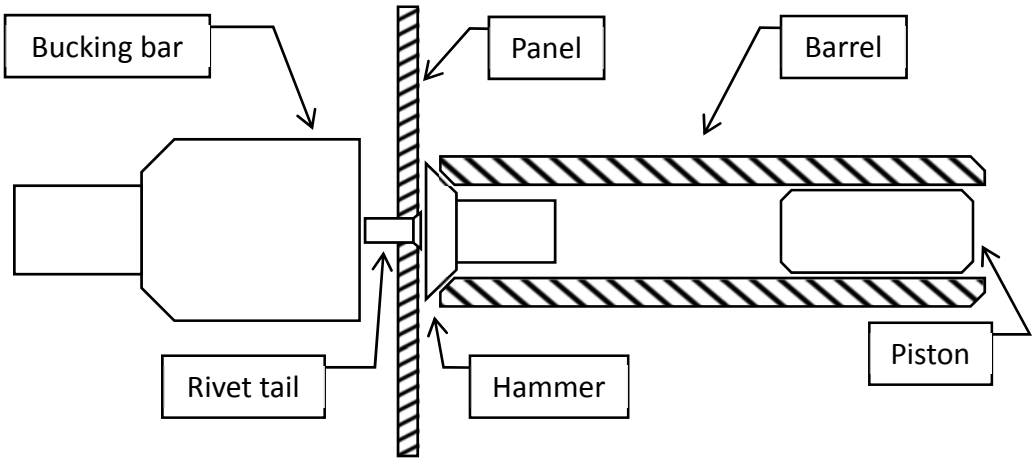

Figure 2.1: Diagram of rivet installation components while piston at is accelerating

After the rivet is inserted into a hole through the panel, the rivet gun is pressed firmly against the head of the rivet. The bucking bar is pressed, initially with less force, against the tail of the rivet. When the gun operator pulls the trigger, compressed air accelerates a piston inside the barrel of the rivet gun towards the back of the hammer. When the piston collides with the hammer, the hammer pushes the rivet toward the massive bar. The inertia of the bar causes it to remain mostly stationary while the rivet is pushed with thousands of pounds against the bar's polished face. The state of the system during the strike is depicted in Figure 2.2.

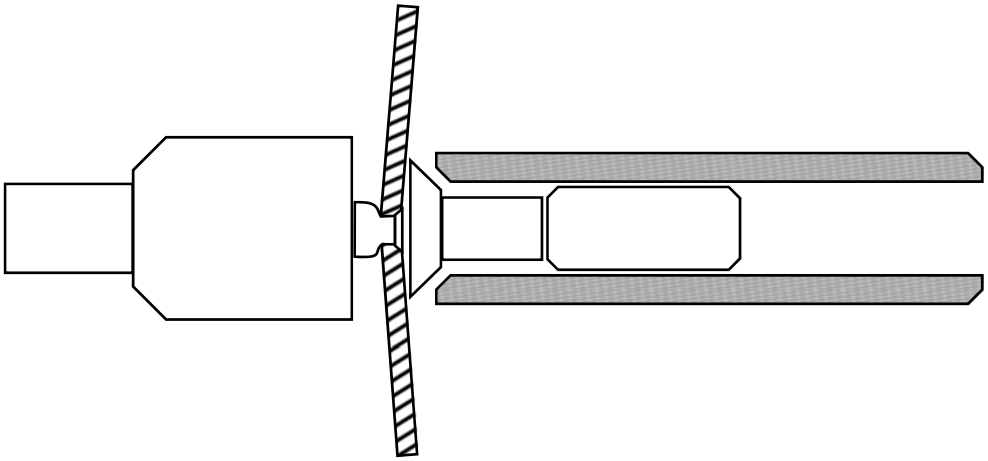

Figure 2.2: Rivet installation components as hammer strikes rivet.

The material inside the hole plastically expands such that what was previously a clearance fit becomes a stronger, interference fit. The rivet tail widens and shortens for a few hundred microseconds until the compression force stops the head from advancing toward the bar. Meanwhile, a shift in air flow in the rivet gun pushes the piston to the back of the barrel for another cycle. The cycle is repeated until the tail of the rivet has progressively deformed to the height and diameter deemed to indicate a sufficient interference fit with the hole.

Note that the head of the rivet facing the rivet gun rests against a countersink in the panel. This prevents the gun from pushing the rivet out of the hole but prevents the head of the rivet from moving toward the bucking bar without moving the panel with it. Therefore, the panel can apply a force on the rivet head which opposes the force of the hammer.

2.2 Momentum and formation rate

We wish to determine how the panel can influence how far the rivet deforms during each hit. Formation continues while the reaction force of the bar is high enough to exceed the yield strength of the rivet. During this time, momentum is flowing from the rivet to the bar at a rate

proportional to that reaction force. The total momentum available to be transferred limits the magnitude of the force applied and the amount of time that force can be sustained. Therefore, factors which limit the total momentum the rivet transfers to the bucking bar during the strike can be expected to also limit the amount the rivet deforms. Conservation of momentum is a natural choice for analyzing collisions and simplifies analysis using Newtonian mechanics.[1]

2.3 Collision dynamics

Let us review the system's dynamics and examine the transfer of momentum within the system. Figure 2.3 is a free-body diagram of the piston, hammer, rivet, and bar.

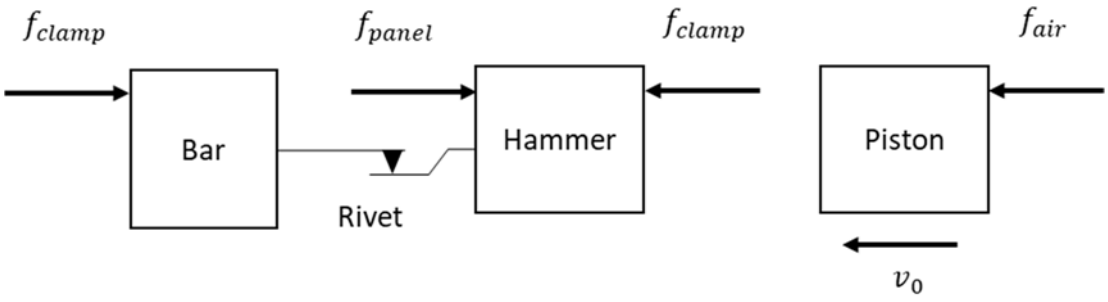

Figure 2.3: Diagram of system of riveting components in direction of axis of rivet

There are four external forces on these bodies in the direction of motion. The "clamp" forces f_{clamp} on the bucking bar and the hammer are applied by the tools' operators to keep the tools in contact with the rivet. Together with the force f_{air} of the pressurized air on the piston,

[1] Lagrangian mechanics would permit an interesting alternative to using momentum transfer as a measure of rivet formation, namely the energy expended to plastically deform the rivet. Work on rivet likely corresponds more closely to amount of rivet formation than momentum. Momentum transferred from the rivet to the bucking bar at forces less than the rivet's yield strength is wasted. Very little energy can be absorbed by the rivet without plastically deforming it. One complication of relying on the proportionality of the rivet's formation to work would be the dependence of the force at yield on the rate of deformation due to the viscosity of the rivet material. Also, an approach which could predict the recoil speed of the piston would likely require an approach considering conservation of both energy and momentum such as in [5]. Ultimately the recoil speed of the piston determines the energy and momentum the transferred to the rivet through the hammer.

these three forces are each on the order of 30-50 pounds. These forces are mostly consistent from each strike to the next, and they are small compared to the collision forces, so considering momentum flow through these forces during the impact itself contributes little to the analysis. We will leave the panel's force on the hammer (through the rivet head) as an unknown force that is possibly the system's primary momentum sink. The rivet is repesented as a massless link that yields at a threshold force (hence the use of a symbol for Coulomb or dry friction here). The hammer and bar have the same, small velocity before the strike, so the bulk of the momentum initially present in the system is in the piston just before impact.

During the impact the piston transfers momentum to the hammer, which immediately transfers momentum to the bucking bar through the rivet at a rate equal to the compressive force of the rivet at yield. Most of the momentum which starts in the piston ends in the bucking bar. But some of the momentum from the piston is instead transferred through the rivet head into the panel at a rate of f_{panel}. Let us examine the piston, the bar, and the panel in turn. Measurements of the initial momentum of the piston and the final momentum of the bucking bar will be useful for assessing the relative amounts of momentum transfer.

2.3.1 Rivet strike: momentum estimate

We can estimate of the momentum output of the rivet gun to be used, the Atlas Copco's RRH 10P TS riveting hammer, from the mass and speed of the piston. Mark Kirshenbaum, a fellow BARC researcher, obtained a mass of 118 grams for the piston, or a weight of 0.26 pounds. Kirshenbaum also learned from the gun manufacturer that the velocity of the piston before impact is 9-10 meters per second [7]. If we assume that the piston's collision with the hammer and load cell is elastic, then the velocity of the piston after the collision is equal and

opposite to its initial velocity. Using the upper figure of 10 meters per second, or 33 feet per second, we obtain the following estimate for the momentum transfer to the hammer:

$$J = m\left(v_f - v_0\right) = \frac{W}{g}(2\ v_0) \approx \frac{(0.26\ lb.)}{32.2\frac{ft.}{s}}\left(2\ \left(33\frac{ft.}{s}\right)\right) \approx 0.53\ lb.s \qquad (1)$$

The momentum output of the Atlas-Copco 10P rivet gun was also measured by firing the tool for thirty strikes (about one second) against a PCB ICP® 200B50 shock load cell stiffly supported by a 0.75-inch thick plate. The force of each pulse was measured at a rate of 200,000 samples per second. The mean of these pulses is shown in Figure 2.4.

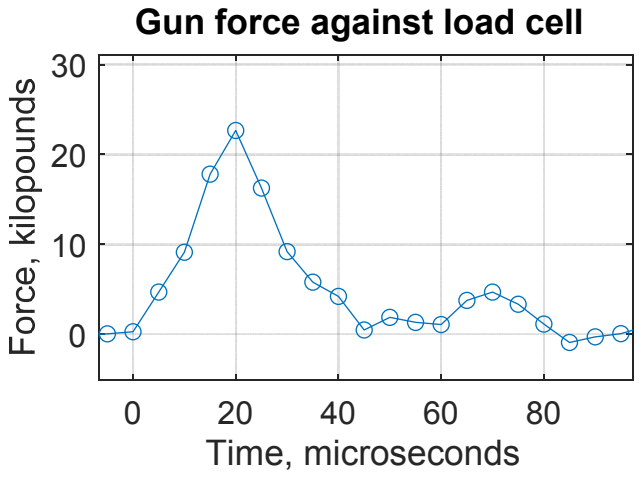

Figure 2.4: Force of rivet gun against load cell semi-rigidly mounted, average of 30 strikes

A triangular impulse of 0.44 pound-seconds appears for most strikes. The pulse is consistently followed 50 microseconds later by a 0.9 pound-second pulse to bring the total to 0.53 pound-seconds. Though this matches the estimate in Equation 1, it is not otherwise clear that the second pulse should be included or that the upper limit of the piston speed should be used. Both estimates are likely to be high.

2.3.2 Bar reaction: Force measurement

The amount of momentum transferred from the rivet to the bucking bar can be estimated by moving the load cell from the rivet gun hammer to between the bucking bar and the rivet. We expect the peak of this force to be slightly greater than required for the stress in the rivet to exceed the rivet's yield strength in compression. Using a yield strength of 7050 aluminum typical for aerospace applications, 61 ksi, a 7/32" diameter rivet yields at 2200 lb.

A single rivet was formed in 11 hits with this arrangement, using the same 10P rivet gun. The peak forces for the hits ranged between 2000 lb. and 3000 lb. The peak forces higher than the predicted 2200 lb. were observed for later hits, showing that rivet tail strengthened as it work hardened and as its diameter increased. The mean of these 11 hits is shown in Figure 2.5. The momentum transferred from the rivet to the bucking bar with each strike, estimated by numerically integrating the force with respect to time over the duration of the impulse,[2] is shown in Figure 2.5.

[2] An estimate of the bar's momentum from the bar's recoil velocity did not corroborate with this number, indicating instead that the bar received 0.6-0.9 slug-feet per second from the rivet. This figure is clearly incorrect; the parabolic fit to the bar position measurements from which this estimate was obtained indicated an acceleration averaging twice that expected for the 35 pound clamp force this experiment. It is not clear what could have caused this discrepancy.

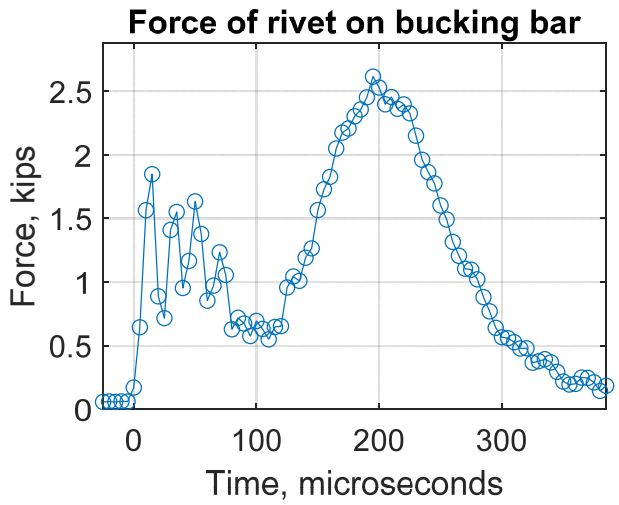

Figure 2.5: Force of 7/32" rivet on bucking bar, average of 11 hits[3]

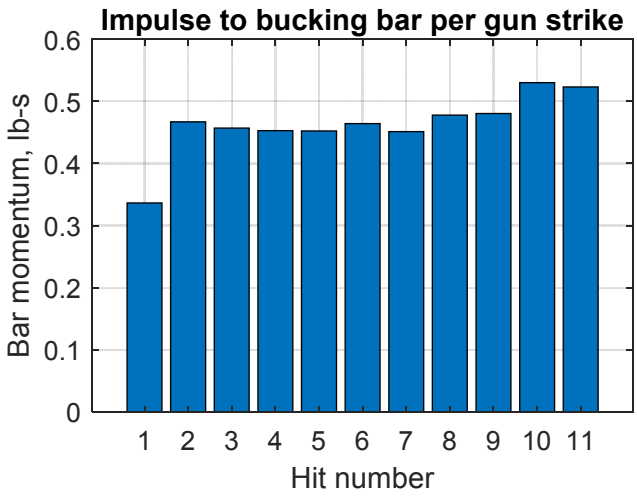

Figure 2.6: Momentum transferred to bucking bar during each of 11 rivet strikes

The momentum estimates were highest for the last two hits, just short of the 0.53 pound second which was estimated for the rivet gun's output. For earlier hits except the first, the

[3] An initial oscillation in the force measurements was observed for all hits after the first. The frequency of this oscillation, about 50 kilohertz, is close to the estimated natural frequency of the load cell. Possibly this oscillation is resonance of the sensor. It is also possible this is the shock wave repeatedly reflecting off the two ends of the bucking bar.

momentum averages 0.46 pound-seconds. It appears that less momentum is transferred to the bucking bar when the rivet is soft. This is likely in part due to the piston transmitting less momentum to the rivet – the initial softness of the rivet reduces the elasticity of the rivet gun's piston's collision with the hammer and rivet. Another likely cause for the reduced momentum transferred in earlier hits is momentum absorbed by the accelerating coupon. For the rivet tail to in length with each hit, the head of the rivet must move towards the bucking bar, bringing the panel with it.

2.4 Impedance types

Momentum flows into the panel in proportion to the force with which the panel resists motion. Broadly speaking, the panel's inertia and stiffness are the two types of mechanical impedance by which the panel resists motion. These components are conceptually illustrated in Figure 2.7.

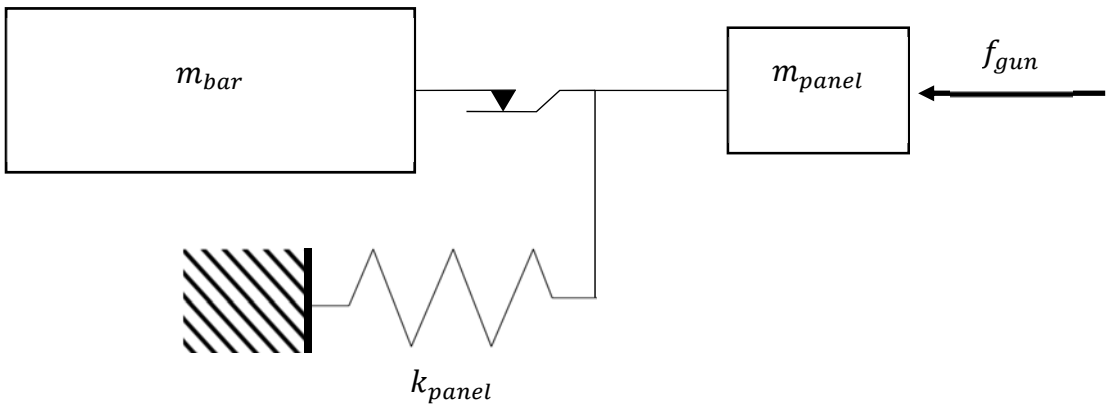

Figure 2.7: Diagram of momentum-absorbing components of system.

2.4.1 Momentum absorption - inertia

When the rivet stops plastically deforming, the panel and bucking bar are no longer moving with respect to each other. These entities have mass, so the final momentum remaining in the system depicted in Figure 2.7 is split between these two bodies. Given that the velocities of the two bodies are equal, the total momentum J_{final} is split between the two bodies in proportion to their respective masses, as described in equation 2.

$$J_{final} = m_{bar}v_{final} + m_{panel}v_{final} = J_{bar} + J_{panel} \quad (2)$$

This momentum absorption by the panel's inertia is largest with a massive panel and a light bar. Therefore, selecting a lighter bar for an experiment studying this effect will make the effect of the absorption easier to observe.

2.4.2 Momentum dispersion - stiffness

The panel is attached with some rigidity to a supporting structure, further resisting motion. The panel can deflect elastically like a spring, but such a spring force siphons momentum out of the system. The rate of momentum flow is proportional to the stiffness of the system and the amount of deflection.

Note that for much momentum to leave the system, the panel must not only be stiff but also sustain a large deflection for some time. Because the collision takes little time (less than 400 microseconds), the amount of momentum diverted by the force of the support structure may not be substantial.

2.5 Plate bending

The spring-mass system presented in Figure 2.7 is very simplified, since the panel is a continuous structure. The next most useful model of the structure is as a thin plate supported at one or more edges by stiff ribs or spars. This model is depicted in Figure 2.8.

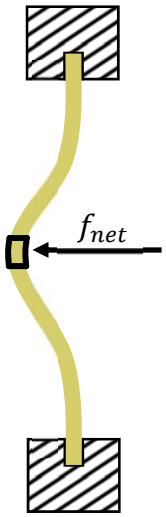

Figure 2.8: Panel/coupon modelled as flat plate, rigidly supported on two edges. Note figure is a cross-section of a two-dimensional domain.

An equation of motion for the plate allows us to hypothesize relationships between the momentum diverted and the plate's qualities. Influential qualities are candidates for factors to vary when testing the panel's effects on rivet formation.

2.5.1 Equation of motion

We will use an equation of motion for the plate which focuses on bending moment. The thickness and deflection of the plate are small relative to its length, so we will assume bulk compression, shear deformation, and rotary inertia can be ignored. Under these assumptions, the motion of a single element in the plate governed by the following equation of motion [8][9]:

$$D\nabla^4 u + m\ddot{u} = f \tag{3}$$

D – plate bending stiffness

u – deflection of the element normal to the plate

m – mass per unit area

f – net force per unit area on the element (in this case, $f_{gun} - f_{bar}$)

Equation 3 is a partial differential equation, fourth-order in space ($\nabla^4 u$) and second-order in time ($m\ddot{u}$). Modelling the plate's behavior during the rivet strike numerically would be informative but is not needed to identify qualities of the panel which may be factors in momentum flow to test. Equation 3 is effectively a force balance equation for a small element of the panel as depicted in Figure 2.9.

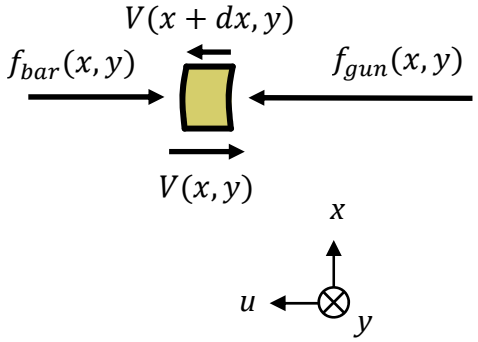

Figure 2.9: Free-body diagram of element of panel, with tool forces and shear forces (V)

As a force balance equation, equation 3 is a momentum flow rate equation, with the right-hand side of the equation describing the element's momentum source and the two terms on the left-hand side describing the element's momentum sinks.

$f = \dot{J}_{in}$:

The difference f between the force of the rivet gun and the force of the bucking bar is the net external force on the element per unit of area. This term describes

the rate of flow of momentum into the element that is not transferred to the bucking bar.

$m\ddot{u} = m\dot{v} = \dot{J}_{absorb}$:

The rate of change of element's velocity is the rate of change of the element's momentum per unit of area.

$D\nabla^4 u = dV = \dot{J}_{shear}$:

The remaining term in equation 3 is the net shear force the element experiences from neighboring elements. It depends on a fourth-order spatial derivative of the element's deflection and on the panel's bending stiffness. The net shear force that an element exerts on its neighbors is the rate at which the element disperses momentum into the surrounding panel.

2.5.2 Coupon factors

We wish to examine how these terms depend on the qualities of the panel to identify quantities which affect the amount of momentum the element absorbs or disperses. The momentum absorption term $m\ddot{u}$ contains mass per unit of area, which is simply the product of the panel's density and its thickness. Knowing the total momentum absorbed requires integrating the momentum absorption over the area of the coupon which moves while the rivet forms. This area depends on the stiffness of the panel.

2.5.2.1 **"Dome" concavity**

The flexibility of the panel should allow it to form a dome with the rivet at the apex. The elements immediately around the rivet move with the rivet while the motion of other elements decreases with increasing distance from the rivet. The momentum dispersion term $D\nabla^4 u$ governs

this behavior. The factor $\nabla^4 u$ s the multi-dimensional analog of the fourth derivative of deflection of a beam with respect to space, or a second derivative of concavity in space. This derivative expresses how rapidly the panel transitions from concave away from the rivet tail near the rivet to concave toward the rivet tail on either side (see Figure 2.10.)

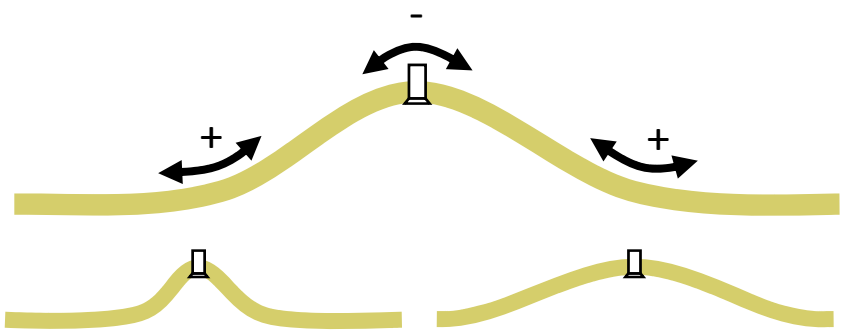

Figure 2.10: Dome-shaped deflection of panel during impulsive loading. Top: dome with highlighted regions of negative and positive concavity. Lower left: small dome permitted by large second derivative of concavity in space. Lower right: large dome due to high plate bending stiffness.

A small dome (lower left panel in Figure 2.4), where only a small area of the panel moves with the rivet, exhibits rapid change of concavity with radius. In a coupon with higher plate bending stiffness D, such a shape would require that the elements nearest the rivet exert a high net shear force (equal to $D\nabla^4 u$) on neighboring elements. These elements move as well, causing the dome to expand (lower right panel in Figure 2.4).

2.5.2.2 **Bending stiffness**

This behavior corresponds to our understanding of $D\nabla^4 u$ as a momentum dispersion term and $m\ddot{u}$ as a momentum absorption term: a higher shear force of the material containing the rivet disperses momentum into a larger area of the panel. The large area implies moves more mass is absorbing momentum by moving with the rivet. Therefore, the mass involved in momentum

absorption increases not only with the density of the panel, but also with the plate bending stiffness D defined in Equation 4.

$$D = \frac{Eh^3}{12\,(1-\nu^2)} \tag{4}$$

E – modulus of elasticity

h – thickness of panel

ν – Poisson's ratio[4]

A high modulus of elasticity thus increases the effective mass of the panel, as does a low value for Poisson's ratio. It is now clear the thickness of the plate increases the area of the dome as well as increasing the panel's mass per unit area. We can readily conclude that a thicker panel should absorb more momentum than a thinner one.

2.6 Plate edges

So far, we have ignored the edges of the plate. If the rivet is far enough from the edge of a plate, then rivet formation ends before the dome expands far enough to substantially intersect the edge. In this case, the behavior of the plate differs little from an infinite plate with no edges. Therefore, in a flexible panel, such as a very thin coupon, proximity to the edge of the plate may not be a factor in its behavior and momentum flow. With sufficiently stiff panels, where the dome reaches the edge of the panel while the rivet is still forming, the momentum flow towards that edge depends on how that edge is supported.

[4] The plate bending stiffness differs from beam bending stiffness in the presence of Poisson's ratio. This is because in beam bending, the side of the beam in compression is free to expand in the other directions. In a beam shaped like a wide plank, this phenomenon would be visible in the edges of the beam plate bending away from the compressed side of the beam. If this perpendicular bending is resisted, the material will be further compressed.

2.6.1 Rigid boundary

When the dome reaches a supported edge of the coupon, the support resists the motion of the dome. This resistance is proportional to the stiffness and mass of the support – a support which is neither rigid nor massive will allow some motion. By forcing the dome to be narrower, the boundary increases the rate of change of concavity of the plate necessary for the rivet to move and consequently increases the rate of momentum dispersion from the rivet. The shear the support exerts on the panel drains that additional momentum into the supporting structure. Therefore, we expect that rivets near a supported edge of the panel would form more slowly than rivets farther away.

2.6.2 Free boundary

Some edges of the panel intersecting the moving dome may be unsupported, or the dome may intersect a junction with a thinner panel. In the case of testing with a very thick coupon, the coupon may be much stiffer than its supports, such that the deflection at the edges of the coupon is greater than the deformation of the coupon itself. Both a free and loosely supported edges exert less shear force and less bending moment on the panel, such that less momentum flows beyond that edge than would flow in a continuous panel. Less momentum dispersed implies more momentum transmitted to the bucking bar; therefore, we would expect that rivets near an unsupported edge of the panel will form more rapidly.

3 Experiment setup

We have identified thickness of the panel as a likely factor in the momentum absorbed by the panel, as well as proximity from a fixed or free edge of the panel. Our hypothesis is that factors which increase the amount of momentum the coupon absorbs will reduce the rate of rivet formation. This hypothesis was tested by installing rivets under varying levels of these factors, measuring the rivets' formation rates and the amount of momentum transferred to the bucking bar.

3.1 Coupon

3.1.1 Coupon mounting

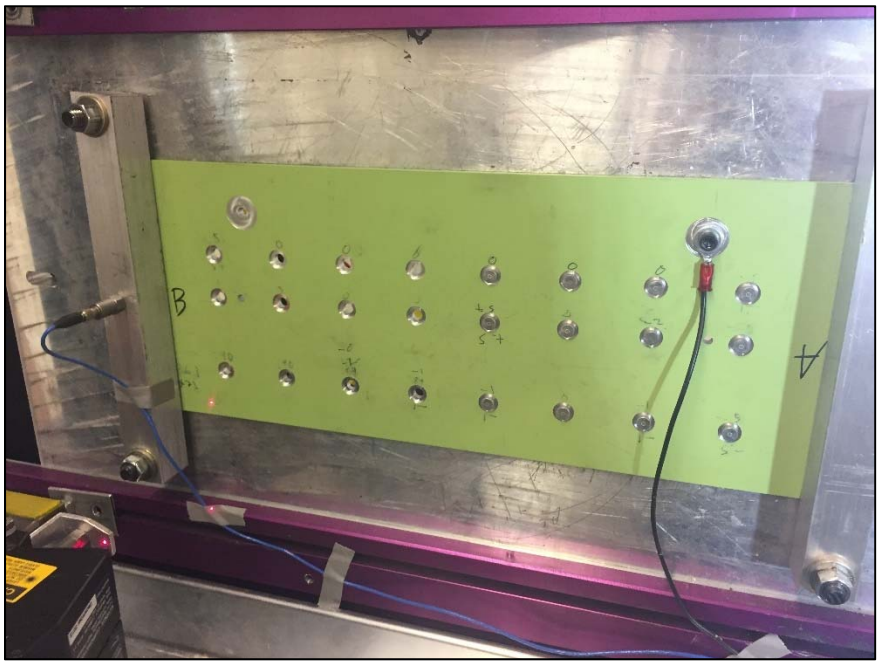

Figure 3.1: Mounted coupon with short edges clamped

The panels tested, shown in Figure 3.1, were 15-inch by 6-inch coupons each supported at its two short edges, leaving the two long edges free. The short edges were clamped to a massive aluminum mounting plate by two of one-inch square aluminum bars with the ends bolted to the mounting plate. A rectangular window cut in the mounting plate admitted the rivet gun access through the mounting plate to the coupon (see Figure 4.3 on page 29). Though the gun-side face of the coupon rested on the plate along all four edges, the two long edges remained free to deflect away from the gun.

3.1.2 Experiment factors

To measure the effects of the thickness of the panel on the riveting process, 24 holes for rivets was drilled in three coupons of different thicknesses.

To measure the effects of a free edge of the panel on rivets near it, the holes in each coupon were arranged in three rows at different distances from the edge. One row was placed as near to the free edge as the rivet gun could reach without colliding with the mounting plate. Another row was placed in the middle of the coupon. The last was placed near the other free edge of the coupon but as near to the rivets in the middle row as possible without those rivets interfering with the bucking bar.

To measure the effects of a fixed edge of the panel on rivets near it, the holes in each row were arranged in four columns on each half of the coupon for a total of eight columns. The first column on each half of the coupon was placed as near to the fixed edge of the coupon as the bucking bar could reach without colliding with the bars clamping the coupon. The remaining six rows were evenly spaced on the coupon such that rivets installed in one column would not interfere with the bucking bar when installing rivets in an adjacent column.

Two rivets were installed at each of the 36 combinations, for a total of 72 rivets. The summary of the factor variations and their values is listed in Table 3.1. The hole pattern used for all three coupons is shown in Figure 3.2.

Table 3.1: Experiment factors varied

Factor	Factor levels				Units	Rivets per factor level*	Expected correlation to formation rate
Thickness	190	250	313		thousandths of an inch	24	-
Distance from free edge	1.2	2	3		inches	24	+
Distance from fixed edge	1.9	3.5	5.1	6.7	inches	18	-

*Some samples omitted from thickest (313) coupon because of process variation

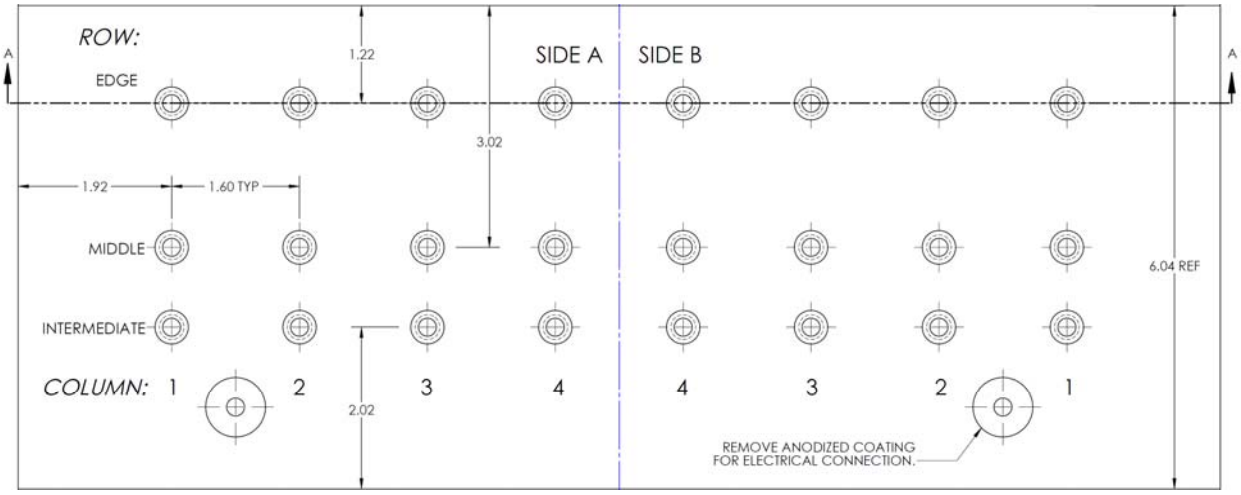

Figure 3.2: Excerpt from coupon drawing showing hole pattern

3.2 Rivets

3.2.1 Rivet grip

This experiment used 7/32 inch diameter, 7-grip rivets. A set of 20 rivets was measured with a micrometer to have a mean overall length of 443.5 thousandths with a standard deviation of 0.26 thousandths, with one outlier of 444.6 thousandths omitted.

A challenge arises with the consistency of the rivet length when attempting to vary the thickness of the coupon. Varying the length of the hole changes the stiffness of the rivet. Additionally, the amount of volume of material from the tail which flows into the panel as the hole expands depends on the length of the hole. Both effects of varying hole length could have effects on formation rate that would then be confounded with the effects of the coupon's stiffness and inertia.

To keep the length of the hole consistent, every hole was counterbored around the rivet tail to offset the thickness of the coupon, as shown in Figure 3.3.

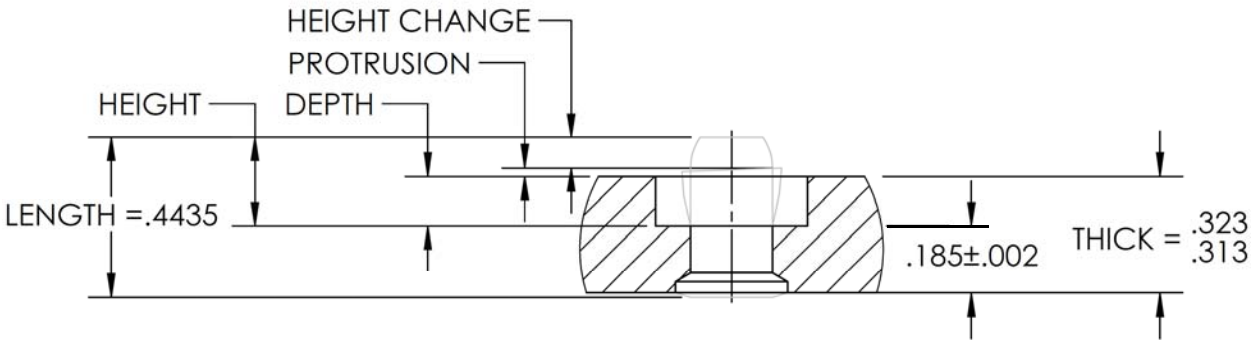

Figure 3.3: Cross-section of hole in thickest coupon. Dimensions in inches. Rivet outlined in gray before and after formation.

This design controlled the length of each hole, such that each rivet tail protruded the same distance from the bottom of the counterbore regardless of thickness. First the holes were drilled,

and countersinks were machined for the rivet head. Then each hole's length was measured by inserting a rivet into the hole and measuring the height of the rivet tail above the surface of the coupon. Then each hole was counterbored to a depth equal to the difference between the original tail height and the target tail height. The target unformed tail height of 250 thousandths of an inch was chosen such that every hole on the thinnest coupon would require a shallow counterbore.

This approach prevented variation in the thickness of the coupon or the depth of the countersink from affecting the hole length and rivet tail height. The only factors in the unformed rivet tail height ("HEIGHT" in Figure 3.3) were error in the depth measurements, variability in the machining of the counterbores, and variability in the lengths of the rivets themselves. Appendix A discusses the small effect these factors may have had on the experiment outcomes.

3.2.2 Button measurement

After all the holes were counterbored, the actual depths of the counterbores were measured. The heights the rivets protruded above the base of the counterbore were also measured. The difference between these two measurements was the height of the tail above the surface of the coupon prior to installation. The height of each tail after installation was compared to each initial height to determine the change in tail height, a metric of the rivet's formation ("HEIGHT CHANGE" in Figure 3.3).

3.2.3 Process duration

All rivets were to be struck with the same number of gun cycles. The number of cycles was chosen such that rivets on the thickest coupon would deform little enough that the tail of the rivet would not sink entirely into the counterbore but still protrude above the surface of the

coupon (“PROTRUSION” in Figure 3.3). If the rivet were struck until tail became flush with the coupon’s surface, the bucking bar would meet the coupon’s surface instead of the rivet, interfering with further formation and thus invalidating comparison of these rivets with those on the other coupons.

4 Experiment procedure

4.1 Test bench

The coupon was mounted to an automated test bench which also operates the rivet gun and bucking bar. Both tools were clamped into 3D-printed carriages, which rode on rails to mobile shelves on the test bench. The rails allowed air cylinders to press the tools against each rivet for installation and then retract the tools after each rivet was completed. A smaller air cylinder mounted on the gun carriage pressed the gun trigger, giving the test bench precise control of how long the rivet gun was active. After each rivet was complete, the air cylinders retracted the tools and servo motors moved the shelves to align the tools with the next rivet. The FESTO pneumatic valve manifold powering the air cylinders, the MOOG Animatics servo motors moving the shelves, and various data acquisition cards were controlled by a National Instruments ™ PXIe 1082 chassis programmed in LabVIEW. Jonathan Ahn describes this same test bench in more detail in [1].

4.2 Rivet gun

The rivet gun used was the Atlas Copco RRH 10P TS. A hammer with a weight of 0.33 pounds was used to drive rivets (a different, 0.287 lb. hammer was used for the two load cell measurements). The gun and hammers are pictured in Figure 4.1.

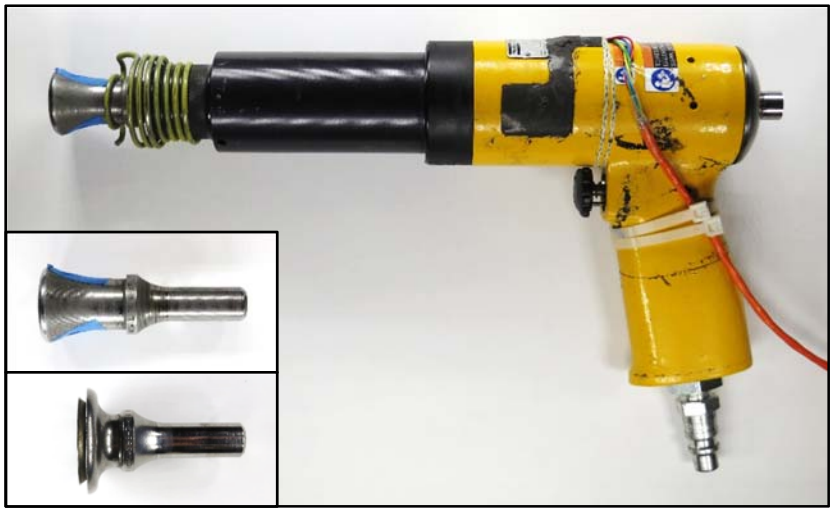

Figure 4.1: Atlas Copco RRH 10P TS rivet gun with .33 lb. hammer (top) and .287 lb. hammer (bottom)

This rivet gun power can be adjusted by rotating the trigger. The trigger was rotated to ~85% power to reduce the clamp force required to keep the bucking bar in contact with the rivet (see Figure 4.2). Specifically, a 0.250” gage rod was used for the spacing between the gun’s barrel and the protruding knob on the trigger to establish the trigger setting. At this power setting the gun operates at 28 Hz.

Figure 4.2: Rivet gun trigger setting, with firing mechanism

The rivet gun was clamped firmly against the rivet with 50 pounds by an air cylinder. The compliant force exerted by the air cylinder allowed the gun to remain firmly seated against the rivet rather than strike it from a distance. This force was sufficient to prevent the bucking bar

from pushing the rivet back out of the coupon towards the rivet gun. The rivet gun carriage and coupon mount plate are pictured in Figure 4.3.

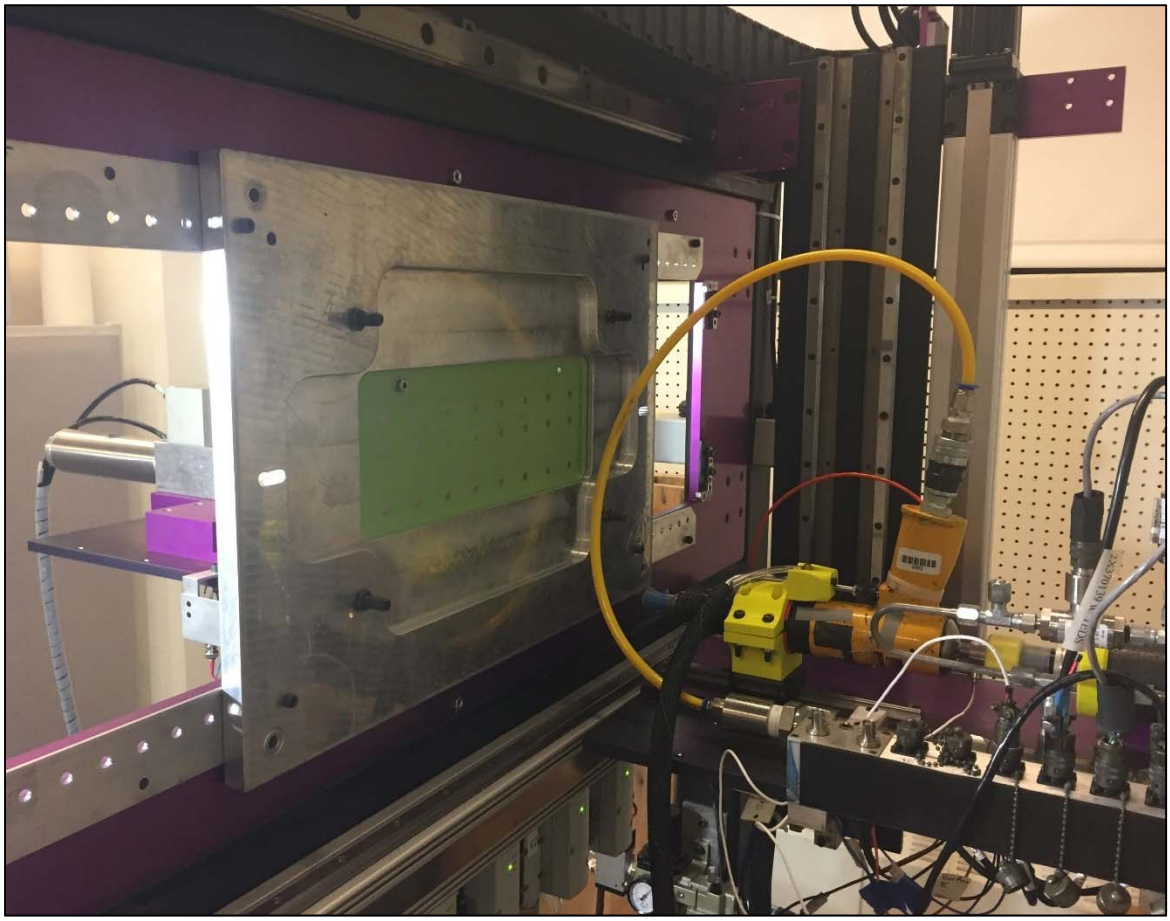

Figure 4.3: Rivet gun mounted in automated test bench

4.3 Bucking bar

A 2.75-pound bucking bar was used with a spring handle. The bucking bar is shown in Figure 4.4 inside a carriage for fixturing; Figure 4.5 is an exploded view of the main components of this assembly.

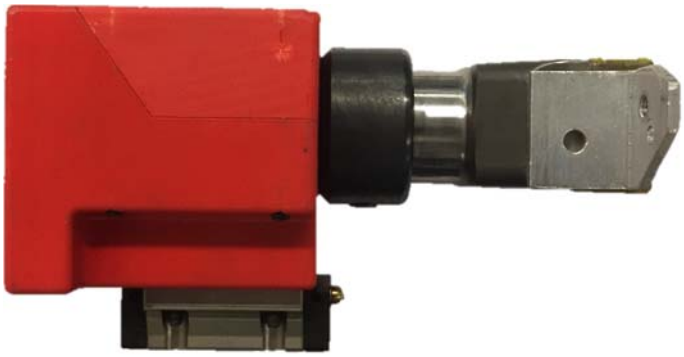

Figure 4.4: Spring bucking bar and carriage assembly

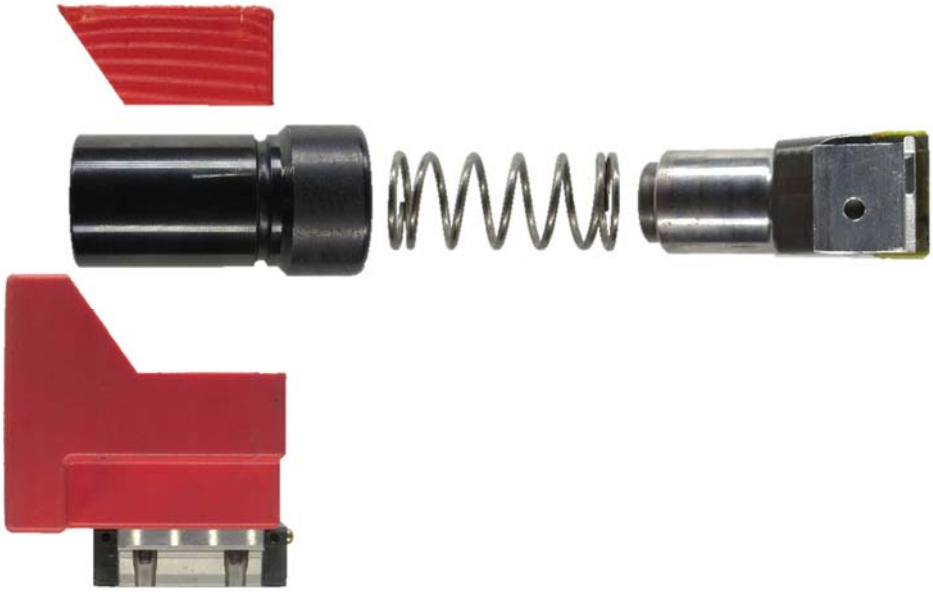

Figure 4.5: Exploded view of spring bucking bar and carriage

The bucking bar was clamped against the rivet with 45 pounds via a spring, with the other end of the spring compressed by an air cylinder. This force was sufficient to return the bar to firm contact with the rivet in time for the next gun strike, but within the range of forces a human operator might be expected to exert. The spring constant was low to keep the force on the bar from changing dramatically during recoil: the 25 pound per inch spring deflected at most

0.25 inches from its equilibrium position, such that the force exerted by the spring varied by no more than 7 pounds. The assembly is pictured in Figure 4.6 and more closely in Figure 4.7.

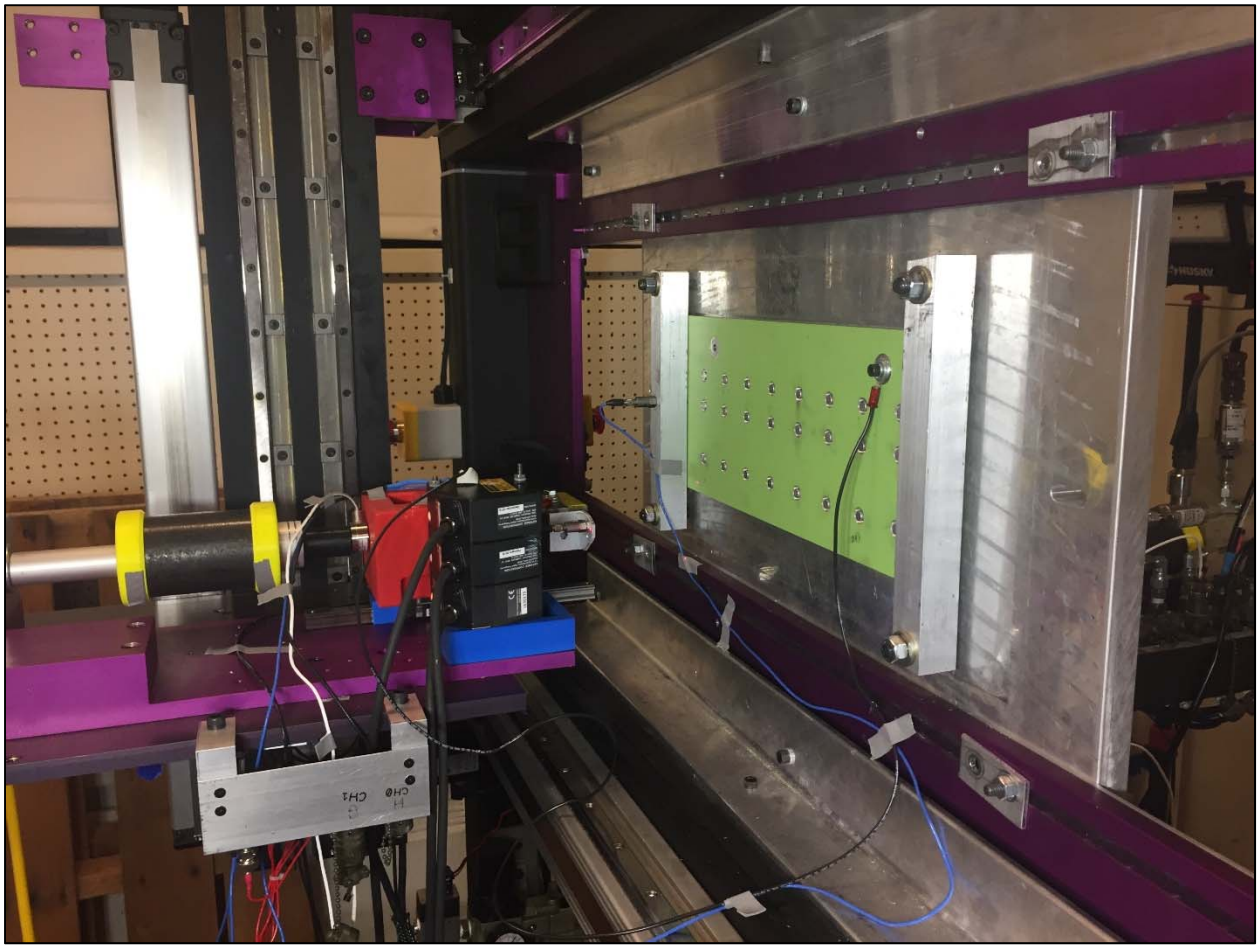

Figure 4.6: View of retracted bucking bar (partially obscured by lasers) and coupon

4.4 Instrumentation

Several instruments on the test bench monitored the tools' behavior during the rivet installation, including bar acceleration, coupon displacement, and gun air consumption. Only the two most informative instruments are described here.

4.4.1 Laser distance measurement

A distance measurement sensor head (Keyence LK-H152) measured the motion of the bucking bar relative to the bar's mounting shelf. The head directed a laser at a fin protruding from the side of the bar and measured the fin's distance from the sensor to a precision of a few ten thousandths of an inch. This sensor permitted monitoring the velocity of the bucking bar during each rivet strike and observe the rivet's height change after each strike. The output was measured at 10,000 samples per second by a National Instruments PXI 6289 card through a BNC 2090 connector block. However, it was discovered after the experiment that the laser controller applied a low-pass filter to the output, with a cutoff frequency of 300 Hertz. The middle of the three sensors depicted in Figure 4.7 monitored the bucking bar while the other two observed the coupon, though low-pass filters on these signals rendered their signals unusable.

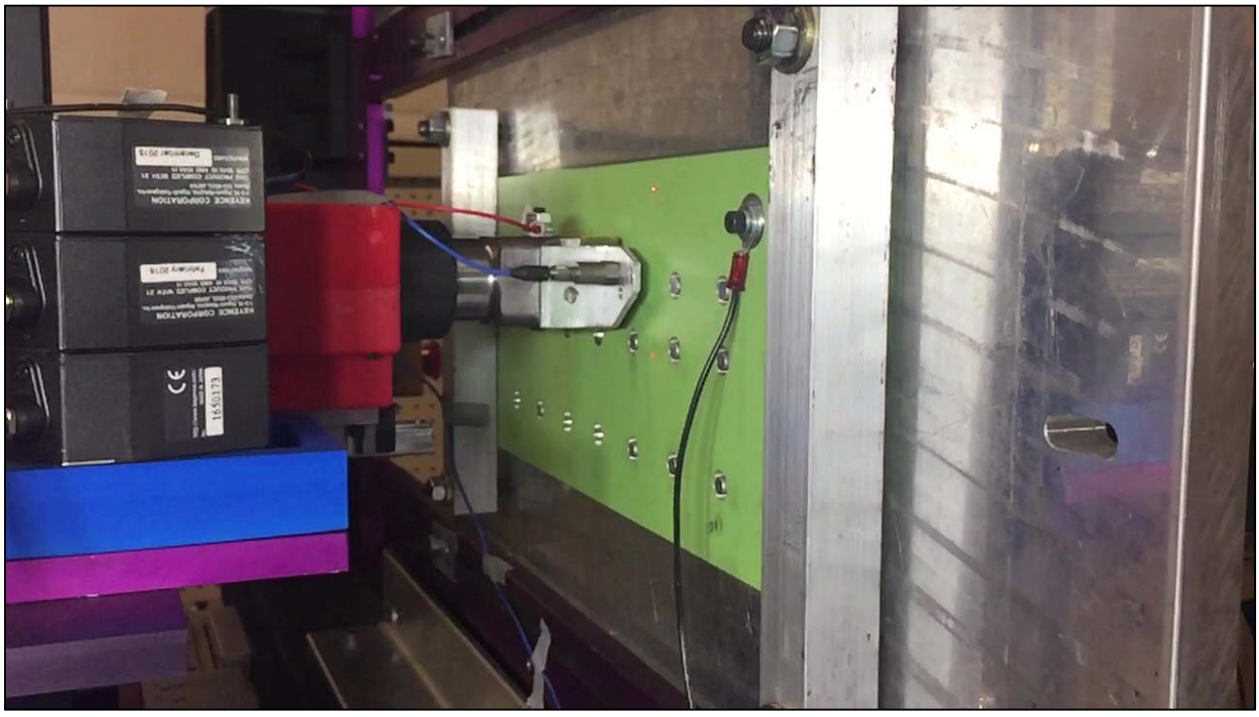

Figure 4.7: Near view of active bucking bar and coupon and Keyence lasers (stack of three)

4.4.2 Contact detector

Contact between the bucking bar and the rivet were determined from the presence of an electrical connection between the bar and the rivet. The bar was electrically insulated from the test bench and from an accelerometer mounted to it, while the coupon was grounded. When the bucking bar was in contact with the rivet, the bucking bar was also grounded. But when the rivet was struck, and the bucking bar recoiled away from the rivet, the electrical connection was broken. A circuit diagram is pictured in Figure 4.8.

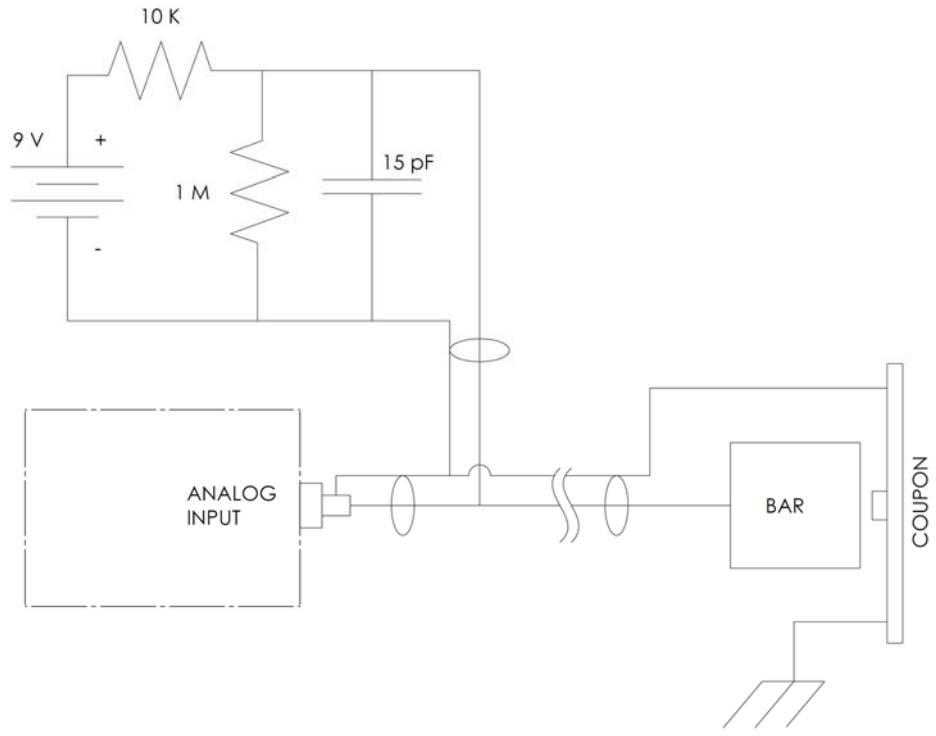

Figure 4.8: Contact detection circuit diagram

A pull-up current from a 9-Volt battery through a 10K resistor onto the bar raised the bar's voltage to approximately 8 Volts whenever the bucking bar was not in contact with the rivet. The pull-up circuit included a low-pass filter with a cutoff frequency of 11 kHz. The

voltage on the bar was sampled 100,000 times per second with an analog input on a National Instruments PXI 6289 card through a BNC 2090 connector block.

The separation of the bar from the rivet appeared as a rise in the bar voltage sustained until the bar returned to contact with the rivet. After the bar returned, an intermittent electrical connection caused the bar voltage to fluctuate. Recoil from gun strikes were differentiated from brief losses of contact by comparing the duration of the contact loss to a threshold time. The beginning and end of sufficiently long periods of high voltage were marked as the times the bar and returned to the rivet, respectively, due to the gun strike.

4.5 Order

Rivets were installed in one half of a coupon at a time. After the twelve rivets on one half of a coupon was done, the coupon was removed from the mount and the next installed. The order in which each half of each coupon was completed was chosen such that any gradual change in the process over time would not be confounded with the effects of the coupon thickness.

Within each half of a coupon, an ordering of the twelve holes was chosen such that any gradual change in the process over time, especially accumulated mass of the previously installed rivets, would not be confounded with either factor of distance from free edge or distance from fixed edge. The same randomized order was used on all six coupon halves. See Appendix B for the ordering details.

5 Data analysis

The metrics for rivet formation were total rivet tail height change and tail height change per hit. The bucking bar's momentum after impact was also estimated from the bar's position. The data was imported into MATLAB for the statistical analysis and figure generation that follow.

5.1 Tail height changes

To measure of the total rivet formation, the final heights of all the rivet tails were subtracted from the initial rivet tail heights, recorded after machining the coupons. Three rivets from the first half of the first, thickest coupon received fewer than seven full strikes from the rivet gun and were omitted from the following analyses. The remaining 69 tails decreased in height by 103.9 thou on average over seven strikes, with a standard deviation of 5.4 thou. Analysis of variance of these changes in each rivet tail's heights indicated which factors had significant effects on the tail heights, i.e., whether any groups' means were statistically significantly different at the $\alpha = 0.05$ significance level.

The analysis of variance rejected the null hypothesis that the means of the tail height changes on the three thicknesses of coupons were equal. The means for rivets on each of the three coupons are shown in Figure 5.1 together with the means for each row, i.e. the variation in tail height changes due to each rivets' distance from a coupon's free edge.

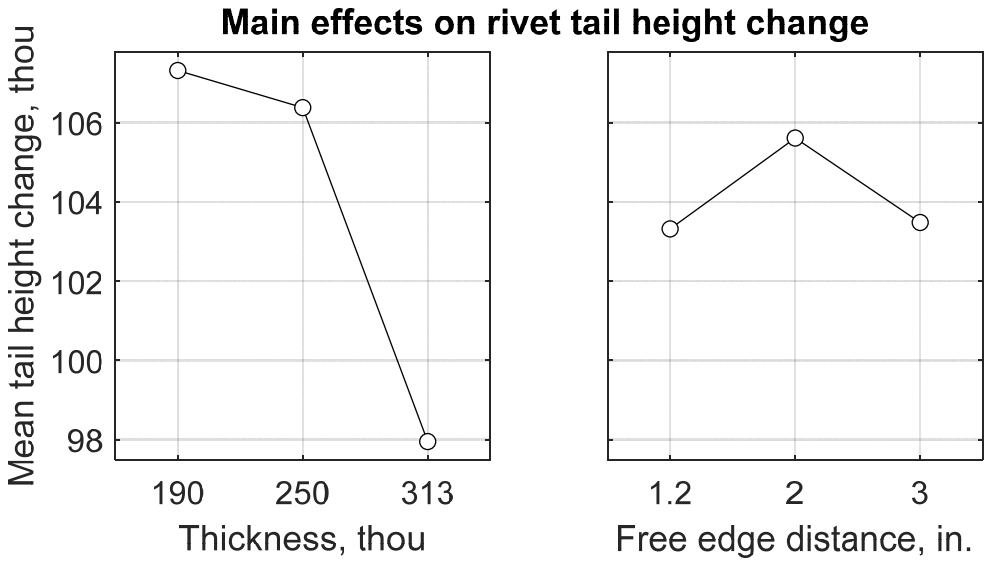

Figure 5.1: Statistically significant main effects on rivet tail height changes

While the effects of coupon thickness were statistically significant by a large margin, the effects of position – distance from free edge and distance from fixed edge – were much less significant. Figure 5.2 shows that on the thinnest coupon, the free edge distance groups had different distributions, but the pattern waned for the thicker two coupons.

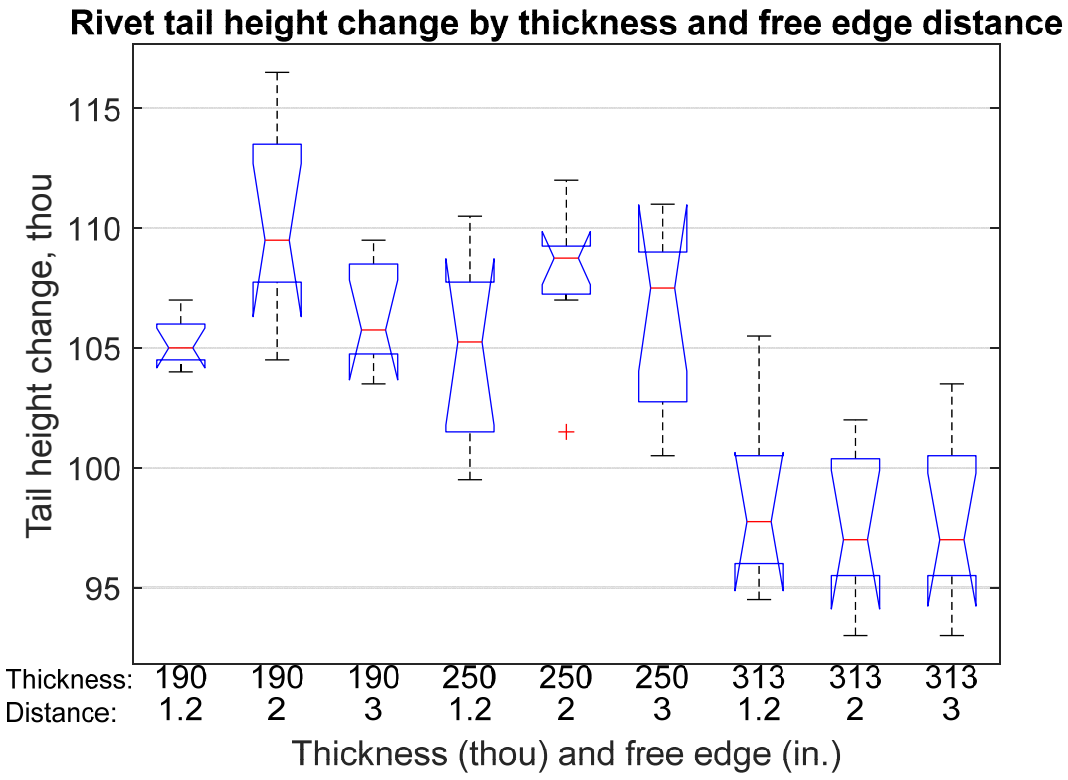

Figure 5.2: Tail height changes by thickness and distance from free edge

The red horizontal lines in box plots such as in Figure 5.2 show the medians of each group of rivets. In this case the rivets are grouped such that all the rivets in a given group are in the same thickness of coupon and are at same free edge distance. The top and bottom ends of each box show each group's 75% and 25% quartiles. The whiskers show the full range of the group, except outliers marked with red "+". The angled notches in the boxes show the confidence interval for the median of the group; groups whose notches do not overlap have statistically significantly different medians at the $\alpha = 0.05$ significance level.

The most statistically difference observations are that all groups on the thickest coupon were less formed than all groups on the two thinner coupons. The mean height change of rivets on the thickest coupon was 8% less than rivets on the other two coupons. This reduction is

consistent with the hypothesis that a thicker coupon inhibits rivet formation by absorbing more momentum, as described in section 2.5.2.2.

The only other observation is that the rivets closest to the edge of the thinnest coupon were different than the two groups of rivets second closest to the edges of the thinnest two coupons, respectively. It was hypothesized in section 2.6.2 that formation rate would decrease with the rivets' distance from the edge of a coupon. The only significant effect of distance from a free edge observed on the thinnest coupons is that the rivets at the extreme distances (nearest the edge or farthest from the edge) formed less than those at an intermediate distance, which is not consistent with the hypothesis regarding free edge distance.

5.2 Recoil momentum

5.2.1 Derivation

Estimating the momentum transmitted from the rivet to the bucking bar during the rivet strike is important to evaluating how closely momentum transfer is related to formation rate. The momentum change of the bucking bar during the gun strike can be inferred from the mass of the bucking bar and the velocity of the bar immediately before and after the strike (equation 5).

$$J = m(v_f - v_0) \tag{5}$$

The velocities before (v_0) and after (v_f) the strike were both estimated from the Keyence laser's measurements of the bucking bar position (section 4.4.1, "Laser distance measurement"). The time of each hit was derived from the contact detection circuit (section 4.4.2, "Contact detector"). Visual comparison of the strike times from the circuit with the laser measurements showed that the laser measurements were delayed by half of a millisecond. The contact start/end times were offset in time to compensate. The contact start/end times were then

used to locate strike times in the position data. An example of the bar position data during one strike is shown in Figure 5.3.

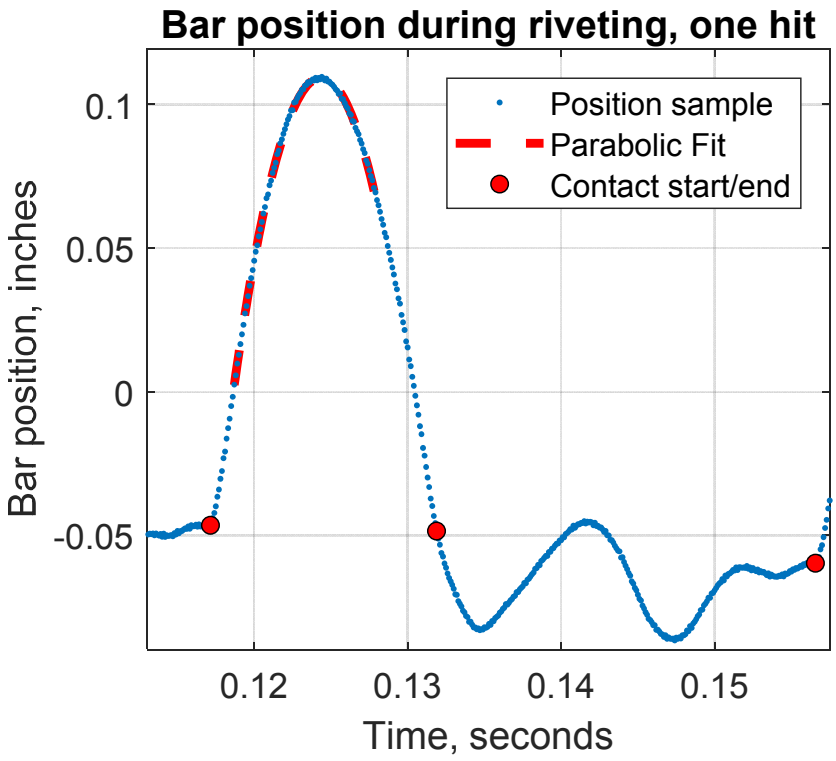

Figure 5.3: Parabolic fit to position of bucking bar during recoil

The velocity of the bar immediately before the time of the strike was assumed to be small relative to the velocity of the bar after the strike. The initial velocity was simply estimated by taking ten position samples before the strike time indicated from the contact data and fitting a line to those samples to obtain the slope. The velocity after the strike was more difficult to obtain due to the 300-Hertz low-pass filter applied to the position data (mentioned in section 4.4.1, "Laser distance measurement"). The low-pass filter smoothed the transition in the bar's motion during the strike, reducing the slope of the position data immediately after the strike.

To better measure the initial velocity of the bucking bar, the bar's motion for several hundredths of a second after leaving the rivet was interpreted as an effectively ballistic trajectory

under the near-constant force the spring exerts on the bucking bar during recoil. A parabolic model fit to a wide section of this trajectory allowed extrapolating the bar's motion back to the strike time without using the position data strongly affected by the low-pass filter there. The start time of the fit was chosen to be after the effects of the low-pass filter on the transition had substantially decayed. The end time of the fit was selected to be shortly after the peak of the recoil. Much later than the peak, the force of friction in the bar's sliding mechanism caused the bar position to substantially deviate from the model fit to before the peak recoil. The model appears as a dashed line superimposed on the data in Figure 5.3. Equation 6 is the model fit to this section of position data x_{bar} in terms of the time t since the strike.

$$x_{bar} = v_0\, t - \frac{1}{2} a t^2 + \epsilon \tag{6}$$

The initial velocity v_0 and constant acceleration a were the parameters obtained from the fit. The velocity v_0 was taken to be the velocity of the bar immediately after the strike to be used in equation 5 for the bar momentum.

One flaw in this approach is that the low-pass filter introduces a time lag in the position data, such that the time between the peak of the parabola and the strike time is inflated by a few tenths of a millisecond. Therefore, the velocity estimates are probably consistently high by a small offset. Fortunately, this offset depends mostly on the acceleration of the bar from the spring force, which was held largely constant over the course of the experiment.

Bar momentum estimates were obtained for each of the seven strikes for each rivet. The bar momentum estimate reported for each rivet was the mean of strikes 4 through 6. These three hits were chosen to be consistent with the use of these hits for estimating the tail height change per hit. This decision is explained in section 5.3.1.

5.2.2 Results

A bar momentum change estimate during each strike was obtained for the same 69 rivets analyzed for tail height change. The mean impulse was 0.390 pound seconds per strike, with a standard deviation of 0.033 pound seconds. Analysis of variance of the bar momentum for each rivet indicated which potential factors in the coupon's momentum absorption had significant effects on momentum transfer at the $\alpha = 0.05$ significance level.

The null hypothesis that the mean bar momentum was the same for each thickness of coupon can be soundly rejected. The average momentum transferred to the bucking bar when riveting on the thinnest coupon, 0.42 pound seconds, is less than the 0.46 pound seconds transferred to a heavier bucking bar in section 2.3.2. This is consistent with the reasoning in section 2.4.1 that the coupon diverts more momentum from a lighter bar. As hypothesized, the momentum transmitted to the bucking bar steadily decreased with increasing coupon thickness. The mean bar momentum for each group, in order of increasing coupon thickness, were 80%, 73%, and 67% of the theoretical maximum momentum output of the rivet gun (0.53 pound seconds) estimated in section 2.3.1.

The effect of distance from the free edge on momentum was statistically significant while the effects of distance from the fixed edge was not. However, the interaction between coupon thickness and distance from free edge was also fairly significant. Rather than display main effects, the nine groups at each combination of coupon thickness and free edge distance are shown in Figure 5.4.

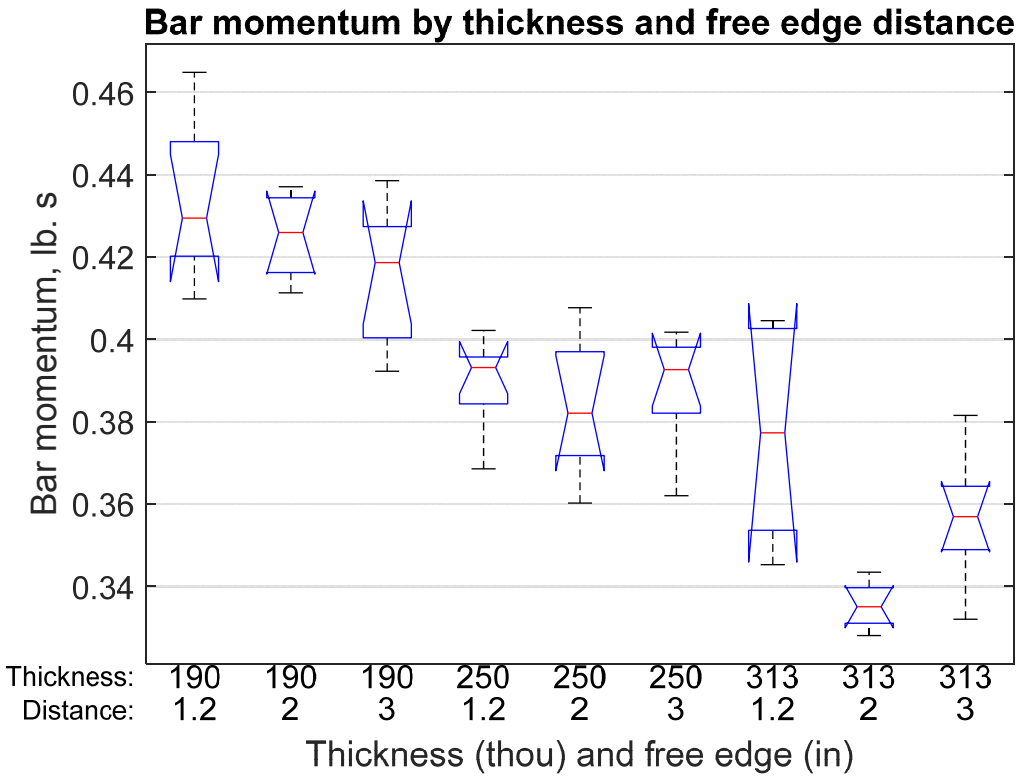

Figure 5.4: Bar momentum by thickness and free edge distance

The variation in bar momentum with free edge is only significant in that on the thickest coupon, rivets two inches from the free edge had the lowest momentum of any group. This result runs contrary to the hypothesis in section 2.6.2 that the group farthest from the free edge ought to exhibit less momentum transfer than the other two. The rivets nearest the free edge of the thickest coupon are also notable in that they varied widely, though the omission of two faulty samples from that group probably inflates the width of that group's confidence interval. Aside from this group, Figure 5.4 shows a clean distinction between the three thicknesses of coupon in terms of bar momentum. This result supports the hypothesis in 2.5.2.2 that thicker coupons absorb more momentum.

5.3 Formation per hit

5.3.1 Derivation

The bar position measurements by the Keyence laser were also used to estimate changes in the rivet tail height. As the rivet tail shortens with rivet gun strike, the bucking bar position while at rest against the rivet moves closer to the coupon. This trend is visible in the net negative trend (toward the coupon) in the example of the bar's position given in Figure 5.5.

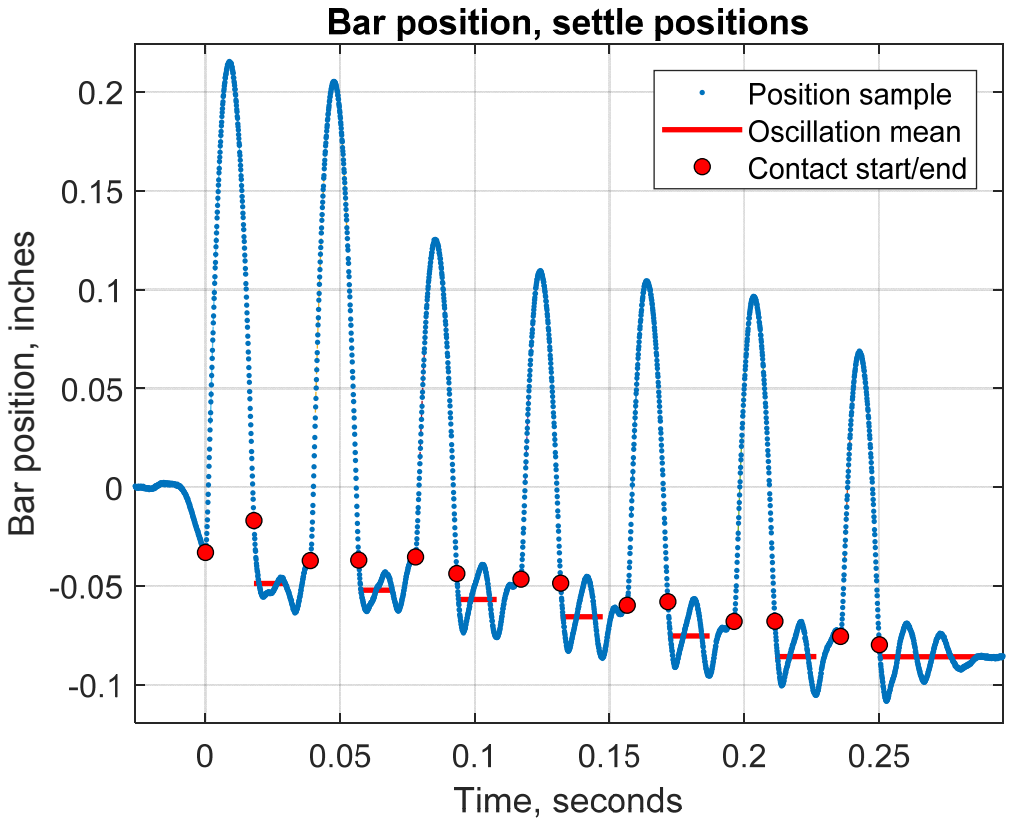

Figure 5.5: Means of bucking bar's settling positions decreasing with rivet formation

While tracking the formation of the rivet with each strike is valuable, there is a challenge with extracting this information from the position of the bucking bar. The rivet and bar are not stationary during that time – the coupon is still vibrating after the strike. Now, the force of the

gun and bar on the coupon are controlled such that the equilibrium position of the bar should be consistent from strike to strike. Therefore, if we could easily extract the mean of a full period of the bar's oscillation, we would have the coupon's constant equilibrium position, offset by the rivet tail height we wish to measure. However, the frequency and phase of this oscillation pattern varies widely from rivet to rivet and even from hit to hit. Consequently, extracting a segment that contains one oscillation cycle is difficult, and the mean of any other segment depends strongly on the oscillation pattern. Fortunately, the pattern which arises after the third hit, though nearly unique to each rivet, tends to persist through sixth hit. The means of these periods for each individual rivet can be compared to obtain the formation over the three hits (the fourth through the sixth). The segment starts at the time the bar contacts the rivet. The segment's end is chosen to avoid the period where the rivet gun begins to accelerate the piston, because the force the gun exerts on the coupon changes during that transition.

5.3.2 Results

The average tail height change during the fourth, fifth, and sixth hits was 9.9 thou per hit. The mean height change per hit for each rivet had a standard deviation across the 69 rivets of 1.76 thou. Figure 5.5 shows the main effects of each factor on mean formation per hit during the fourth through the sixth hits.

Figure 5.6: Main effects on height change per hit, hits 4-6

The null hypothesis that the means of the rivets on each coupon were all the same can be rejected – rivets on the thicker two coupons formed 21% less per hit during the fourth, fifth, and sixth hits than rivets on the thinnest coupon. Variations in the height change per hit with the rivets' position on the coupon are also statistically significant but by a narrow margin. Furthermore, neither pattern follows the expected trends of formation rate decreasing with free edge distance or increasing with fixed edged distance.

As with the total height changes (in section 5.1 on page 35), the height change per hit measurements indicated that rivets on the thinnest coupon formed more quickly than rivets on the thickest coupon. But when considering total height changes, rivets on the middle thickness of coupon were statistically indistinguishable from rivets on the thinnest coupon. The opposite is true when considering height change during the fourth through the sixth hits: rivets on the middle thickness exhibited height changes per hit which were statistically indistinguishable from those of rivets on the thickest coupon.

6 Discussion

6.1 Formation rate comparison

Despite the significance values reported by the ANOVA, it seems unlikely that the effects of position observed here – distance of the rivet from a free edge or a fixed edge of the coupon – would be reproduced if this experiment were repeated. The effects of coupon thickness, however, are not readily dismissed. The quantity of momentum of the bucking bar steadily decreased with increasing coupon thickness. Both metrics of formation rate – total change in tail height and average change in bar resting position per hit – indicated that rivets formed more slowly on the thickest coupon than on the thinnest.

These two metrics disagree, however, on the formation rate of rivets on the middle thickness coupon. These rivets formed as slowly during the later hits as rivets on the thickest coupon yet achieved the same final height as rivets on the thinnest coupon. Another point of disagreement between these formation rate metrics is in the magnitude of the effect of thickness. Total height changes varied by 8% of the thickest coupon while height changes during later hits varied by 21% of the thickest two coupons. This discrepancy suggests that these two means of measuring of formation rate are not actually measuring analogous quantities.

Indeed, when we plot the two metrics against each other, the positive correlation we might expect to see between these metrics is completely absent! No relationship between the two metrics is visible until we distinguish between measurements on each thickness of coupon, as is done in Figure 6.1.

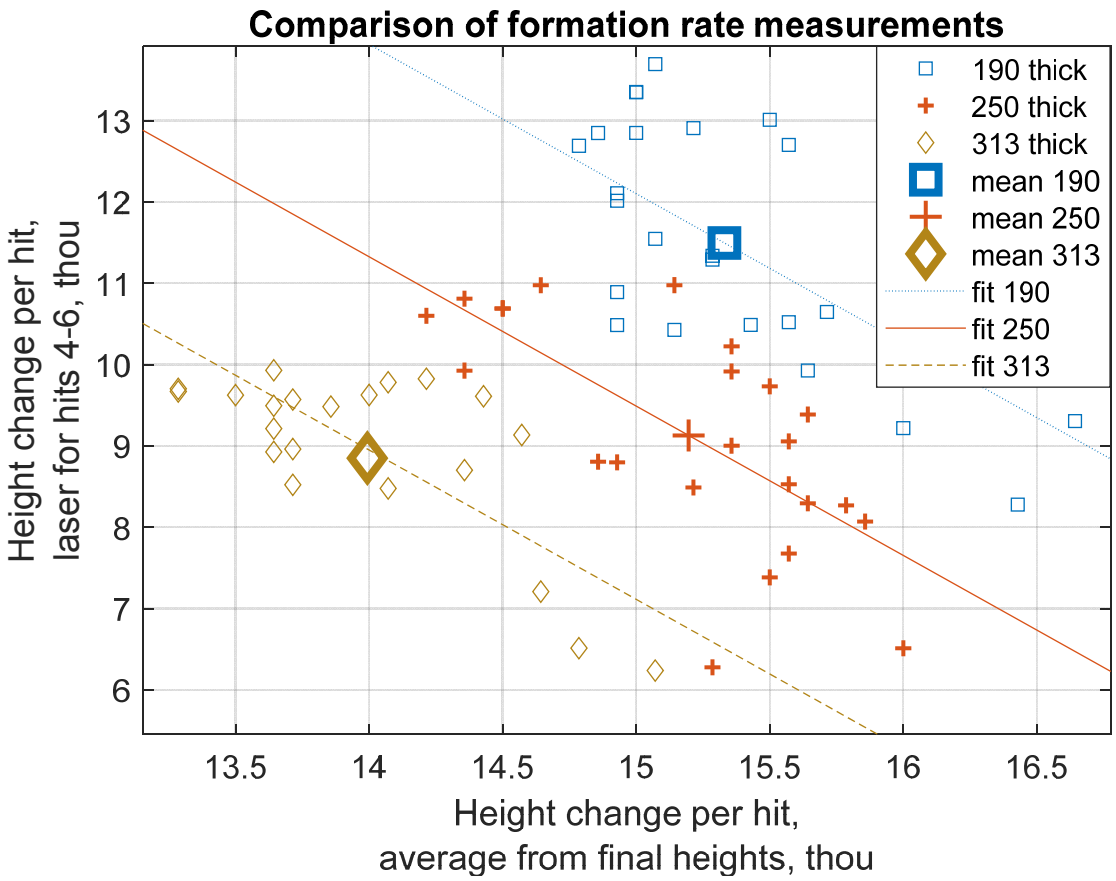

Figure 6.1: Comparison of formation rate measurements

Each small marker in Figure 6.1 shows a single rivet, with the average height change over seven hits plotted on the horizontal axis and the average height change over the fourth, fifth, and sixth hits plotted on the vertical axis. The shape and color of each marker corresponds to the thickness of coupon in which the rivet was installed. The three large markers are the means for each thickness of coupon. With the means for each thickness, Figure 6.1 shows what we have already observed for each metric individually. The measurements from final heights agree with the measurements from bar position that rivets on the thinner coupon formed faster, but the measurements disagree on where to place the group of rivets on the middle thickness.

The shape of each thickness group shows that the groups are quite distinct, strengthening the hypothesis that thickness of the coupon affected formation rate. The shapes of each group also suggest that a correlation exists between the two metrics, and that the correlation is the consistent across the three groups – we can fit the same slope of line to each group simply by changing the intercept. Strangely, that correlation is negative – rivets which formed more in three of the last four hits tended to achieve less total deformation!

6.2 Rivet strengthening and formation rate

Chance or measurement error cannot readily explain the negative correlation between these two quantities – total tail height change, observed from the final tail heights, and height change per hit, observed from the bar position during the fourth through the sixth hits. A more likely explanation is from the mechanics of rivet formation: rivets form more slowly the farther they progress.

The rivet tail widens as it is struck, increasing its cross-sectional area in proportion to the square of its diameter. This greater area inevitably increases the compressive force needed to create stresses in the tail exceeding the material's yield strength. Additionally, the deformation causes the rivet to work harden, increasing its yield strength. Therefore, we can expect that the rate of formation slows down as formation progresses.

The likelihood that a rivet forms more during the first three hits than the next three hits is apparent from a comparison of the two sources of tail height change data: the average rivet formed a total of 104 thou during all seven hits, but only a 30 thou of that formation occurred during the fourth, fifth, and sixth hits. This leaves 74 thou of formation occurring during the first three hits plus the final, seventh hit. This implies about 5/7 of the formation occurred during 4/7

of the hits. Now suppose the rivet is no softer during the seventh hit than the previous three, and then assume the rivet also deforms 10 thou during that hit. Under this assumption, we would attribute 21 thou of deformation on average to each of the first three hits, and only an average of 10 thou to each of the final four hits. Thus far the difference between initial formation rate and later formation rate fits well with our data.

To illustrate how the strengthening of the rivet with formation can explain the negative correlation between total and late formation, imagine a race between two rivets. Three snapshots of this race are superimposed in Figure 6.2: first of the rivets' initial heights, then of their heights after three hits, then of their heights at the end of seven hits.

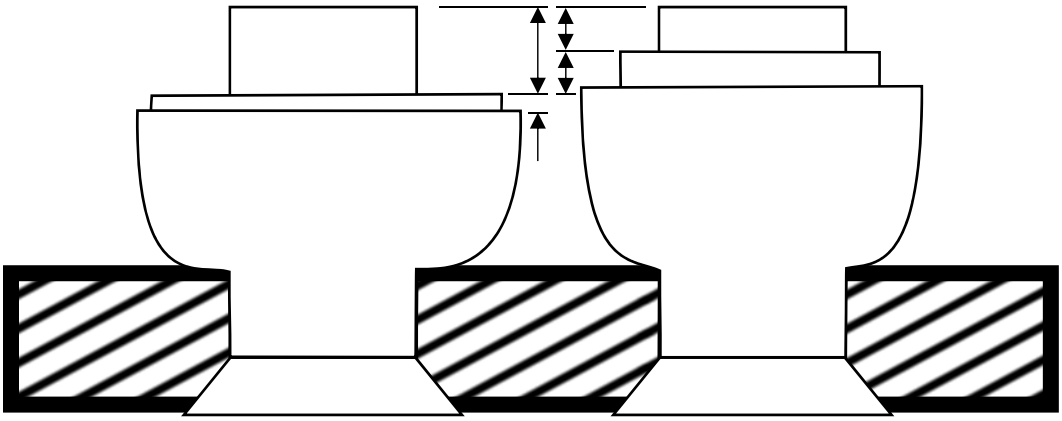

Figure 6.2: Illustration of initial vs. late formation rates

Suppose that during the first three hits, the left rivet happens to form more than does the right rivet. Now the left rivet is wider and stronger and more difficult to further form than the right rivet. At this point in the race, we begin to measure the rates of formation from the bucking bar position. We find during the next three hits that the right, softer rivet forms more quickly than the left, stronger rivet. The right rivet nearly catches up to the left rivet, but as it nears the

left rivet in height it also nears it in strength, preventing it from continuing on to overtake the left rivet. When we measure the final heights, the left rivet still formed more in total than the right.

Returning to the inverse correlation between average formation rate and late formation rate in Figure 6.1, we now have an explanation for this unexpected relationship. Within each coupon thickness, the rivets varied widely in the amount they formed during the first three hits, and this variation dominated the total formation observed in the final rivet heights. This variation also, by varying the rivets' strength, strongly influenced the formation rate during the next three hits. The effect of initial formation was positive on total formation but negative on late formation rate, resulting in the negative correlation between total and late formation.

The reason why the rivets varied so much in initial formation is not clear. We can attempt to explain the behavior of the rivets on the middle thickness coupon: if these formed more initially than rivets on the other two coupons, then their strength would slow them to the same speed as the rivets on the thickest coupon during later hits. Meanwhile, they would fall behind rivets on the thinner coupon because of their strength and their thicker coupon. The question remains, however, why the rivets on the thinnest coupon did not form more during the first three hits than rivets on the middle thickness did.

6.3 Adjusted formation rate

Now that we have identified the strengthening of the rivet as a substantial factor in the variation of formation rate, we can better isolate the factor in which we were originally interested – momentum absorbed by the coupon. Equation 7 is a linear model linking variation in formation rate to variation of the rivet strength and momentum absorption.

$$\Delta h_i = \overline{\Delta h_i} + \beta_h\left(h_{f,i} - \overline{h_f}\right) + \beta_J(J_i - \bar{J}) + \epsilon_i \tag{7}$$

Δh_i – mean tail height change per hit over hits four through six for the i-th rivet, an indicator of formation rate ($\overline{\Delta h}$ is the mean of Δh_i for all rivets)

$h_{f,i}$ – total height change over all seven hits for the i-th rivet, an indicator of rivet strength at the third hit ($\overline{h_f}$ is the mean of $h_{f,i}$ for all rivets)

J_i – mean bar momentum change per hit over hits four through six for the i-th rivet, an indicator of the coupon's momentum absorption ($\bar{J}$ is mean of J_i for all rivets)

ϵ_i – error associated with measurements of i-th rivet, assumed to be normally distributed

β_h, β_J – parameters fitted to the relationships of final height and bar momentum, respectively, to height change per hit

After using a least-squares fit to estimate β_h and β_J, we can define a new quantity, adjusted height change per hit. Equation 8 defines this adjustment as subtracting the effect estimated for the total height change from the height change per hit. If we use 8 to eliminate Δh_i from equation 7 and solve for $\Delta h_{adj,i}$ we arrive at equation 9, illustrating that this adjustment should isolate the effect of bucking bar momentum on height change.

$$\Delta h_{adj,i} = \Delta h_i - \beta_h(h_{f,i} - \overline{h_f}) \tag{8}$$

$$\Delta h_{adj,i} = \overline{\Delta h} + \beta_J(J_i - \bar{J}) + \epsilon_i \tag{9}$$

The mean adjusted height change per hit is 9.9 thou with a standard deviation of 2.0 thou. The correlation of adjusted height change with bucking bar momentum predicted in equation 9 is shown in Figure 6.3.

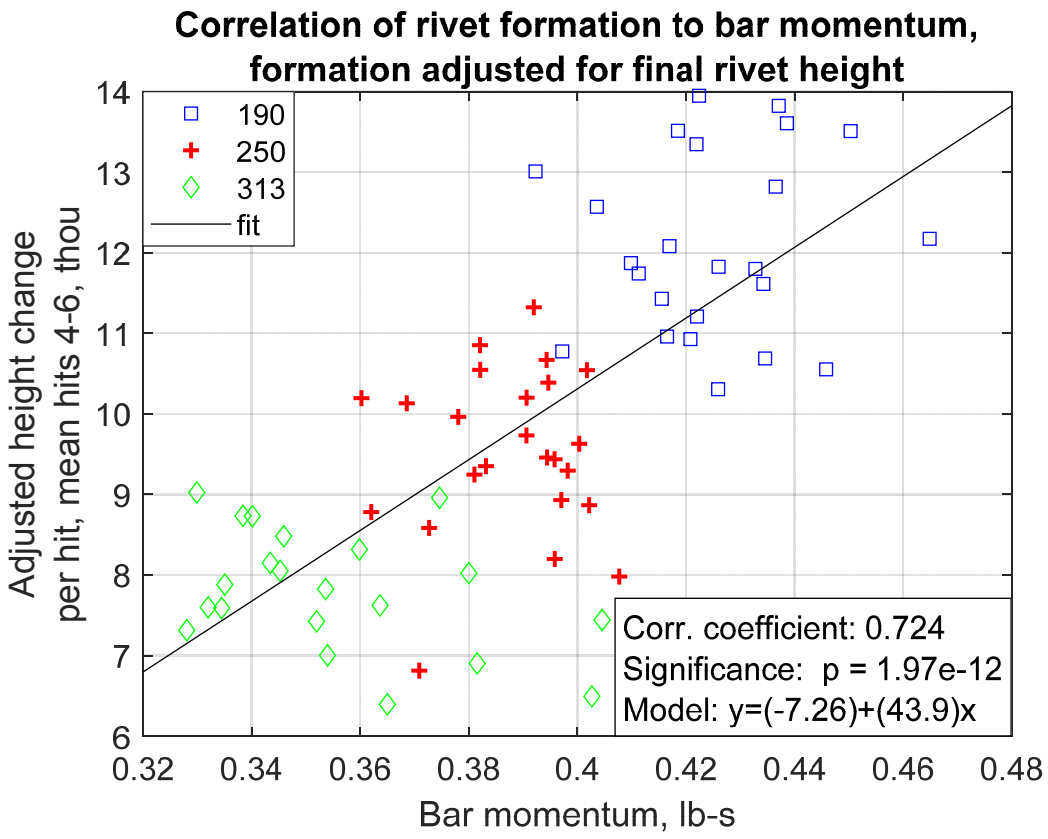

Figure 6.3: Correlation between bar momentum and adjusted height change per hit

The correlation between bucking bar momentum and this adjusted formation rate is statistically significant. The 95% confidence interval for the correlation coefficient is 0.58 to 0.82, indicating a correlation which is not clean but certainly not artificial. The approximate slope of this relationship is 44 thou per pound second. The 18% variation in bar momentum caused by the 49% variation in coupon thickness corresponds to a 43% variation in adjusted formation rate.

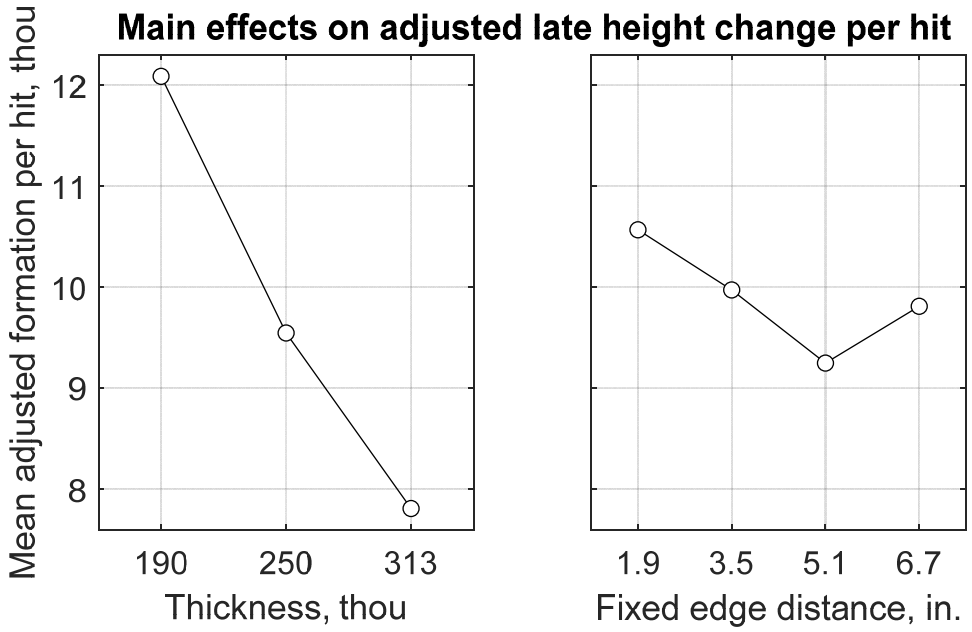

Figure 6.4: Main effects on adjusted formation rate

Figure 6.4 shows the dependence of adjusted height change per hit on coupon thickness is better aligned with the hypothesis of section 2.5.2 than total height change or height change per hit alone. The rivets in the middle thickness of coupon lie between the rivets in the other two coupons rather than being indistinguishable from one group or the other. As hypothesized, rivets on the middle thickness of coupon formed more slowly than those on the thinnest coupon but more quickly than those on the thickest coupon.

The rivets' distance from a free coupon edge did not statistically significantly affect the adjusted height change per hit. A statistically significant variation in the adjusted formation rate appears with respect to the rivet's distance from the free edge of the coupon. The trend resembles the barely significant trend apparent in the original height change per hit, but it is now too significant to ignore. The trend is visible on all three coupons (see Figure C.14 on page 81) that formation rate decreases with distance from the fixed edge of the coupon until except just before

reaching the middle of the coupon. This is opposite the hypothesis that formation rate should increase with distance from the coupon's fixed edge.

6.4 Adjusting for coupon thickness

While this experiment shows that greater coupon thickness reduces bar momentum and formation rate, the correlation between bar momentum and formation rate does not necessarily demonstrate that bar momentum reduces formation rate. Increased coupon thickness does reduce bar momentum, and it appears that reduced bar momentum in turn reduces formation rate, but coupon thickness could reduce formation rate by another mechanism. We can try to disprove this possibility by showing that additional sources of variation in bar momentum cause a corresponding variation in formation rate. The variations needed to see a correlation could be isolated by removing the variations due to coupon thickness, just as we removed variations for rivet strengthening. The corresponding model is equation 10.

$$y_i - \bar{y}_k = \beta_J (J_i - \bar{J}_k) + \epsilon_i \tag{10}$$

y_i – adjusted height change for i-th rivet

$\bar{y}_k$ – mean adjusted height change for the k-th coupon thickness

J_i – bar momentum for i-th rivet

$\bar{J}_k$ – mean bar momentum for thickness k-th coupon thickness

β_J – linear dependence of adjusted height change on bar momentum

ϵ_i – random error for i-th rivet, assumed to be normally distributed

The compensated terms for bar momentum $(J - \bar{J}_k)$ and formation rate $(y - \bar{y}_k)$ are plotted in Figure 6.5. With the variation with thickness removed, the three groups lie on top of each other as desired.

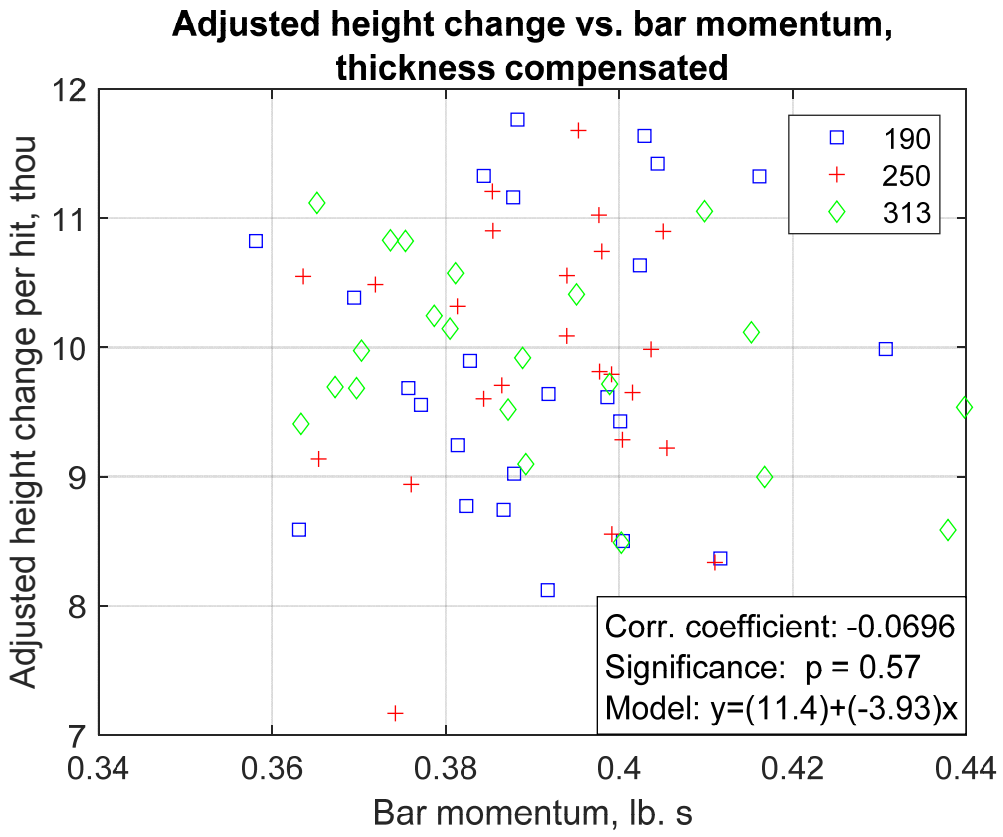

Figure 6.5: Adjusted height change vs. bar momentum, thickness compensated.

Within each thickness, a correlation between bar momentum and formation rate is not visible. Coupon thickness appears to be the only cause of variation in bar momentum which results in a corresponding variation in formation rate. This result suggests that thickness affects formation rate and affects bar momentum, but bar momentum does not affect formation rate.

There is a possible explanation for the lack of correlation between bar momentum and height change per hit, an alternative to the conclusion that bar momentum and formation rate are not directly correlated. The variation in the data observed here is the sum of the variation in the

actual physical quantities (actual momentum and formation rate) and the error in the measurements of those quantities. If the variation due to measurement error is much greater than the variation of bar momentum within each thickness group, the correlation between actual variation in bar momentum and actual variation in formation rate will be hidden. Besides coupon thickness, other sources of actual variation in bar variation are not clear (free edge distance in only the thickest coupon, Figure 5.4 on page 42, and initial tail height from machining variation, Figure A.3 on page 67). So, it entirely possible that the lack of correlation between the measurements shown in Figure 6.5 only describes the lack of correlation between sources of measurement error. While this result fails to prove that a direct correlation between bar momentum and formation rate does exist, it does not necessarily prove that a direct correlation cannot exist.

7 Conclusion

7.1 Momentum discussion

The applicability of percussive riveting tests on surrogate coupons was challenged when one such test indicated that a rivet's formation rate varied dramatically with the rivet's position on the coupon. The hypothesis was proposed that the panel in which rivets are being installed affects the rate of rivet formation because the panel reduces the amount of momentum transmitted to the bucking bar through the rivet. Less momentum transmitted by the rivet's impact with the bar implies less force to deform the rivet or less time for the rivet to deform.

The momentum output of the Atlas Copco RRH 10P TS rivet gun was measured by firing the tool against a shock load cell to obtain a maximum momentum output of 0.53 pound seconds. The shock load cell placed between the rivet tail and a 7.38-pound bucking bar found that 0.46 pound seconds, spread over 300 microseconds, were transmitted through the rivet to the bucking bar with each hit until the final two, when the fully formed rivet transmitted nearly the rivet gun's full 0.53 pound seconds.

It was hypothesized that because the coupon must move with the rivet, the momentum from the rivet gun is split between the coupon and the bar. With a lighter bar, the mass of a coupon is comparatively large enough to absorb a more substantial fraction of momentum from the bar. Because the coupon is flexible, however, only the coupon material immediately surrounding the bar accelerates with the rivet. In a thicker, stiffer coupon the momentum is dispersed to a wider area, increasing the mass that moves with the rivet. Therefore, coupon thickness was proposed as likely a factor in momentum absorption with testing. By this approach, proximity of the rivet to a supported edge of the coupon is also likely to resist rivet

motion by absorbing momentum into the support. Proximity to an unsupported, free edge of the coupon is likely to reduce the coupon's absorption of momentum.

7.2 Experiment procedure

The experiment aimed to test each of these three possible factors in bar momentum and rivet formation – coupon thickness, proximity to a free edge, and proximity to a fixed edge. To vary distance from a free edge, holes were drilled in each coupon in three rows at three different free edge distances (1.2, 2, and 3 inches) and eight columns at four different fixed edge distances (1.9, 3.5, 5.1, 6.7 inches) such that every combination occurred twice on each coupon. To vary coupon thickness without varying the length of the holes, counterbores were machined around the tails of the rivets. Every rivet tail initially protruded approximately the same height above the base of this counterbore, regardless of the thicknesses of coupon (0.190, 0.250, and 0.3125 inches).

The rivets were installed by an automated test bench which held the coupon and pushed the rivet gun and bucking bar against the rivet with 50 and 45 pounds, respectively. The rivet gun used was the Atlas Copco RRH 10P TS. The bucking bar was a 2.75-pound steel head with a spring handle. The test bench automated firing the rivet gun to achieve a consistent seven hits on all but three rivets excluded from the study. The rivets were installed in one half of a coupon at a time in pseudo-random order, and the halves of each coupon were installed in pseudo-random order. A Keyence LK-H152 laser measured the bucking bar motion, and electrical connection between the bar and the rivet permitted precise measurements of the times the bucking bar left or returned to contact with the rivet.

7.3 Experiment results

After the rivets were installed, the total height changes of the rivets were measured, averaging 104.9 thou. Rivets on the thickest coupon formed 8% less than rivets on the other two coupons. The effects of rivet position on total height change were hardly significant nor as hypothesized. The momentum transferred to the bucking bar by the rivet was estimated for a few hits from each rivet by estimating the bucking bar's velocity before and after the hit. The means of the bar momentum for rivets on each thickness of coupon, in order of increasing thickness, were 80%, 73%, and 67% of the theoretical maximum output of the rivet gun. Variation in bar momentum with free edge distance was significant in the thickest coupon but also not in the fashion hypothesized. The rivet's height change per hit was estimated from the change in the resting position of the bucking bar when in contact with the rivet, though due to the rivet's vibration this could only be reliably done for the fourth, fifth, and sixth hits. Height change per hit averaged 9.9 thou, with the rivets on the thicker two coupons forming 21% less per hit than rivets on the thinnest coupon. The effects of position were neither decisively significant nor as predicted.

The total height change per hit and the late height change per hit were found to be negatively correlated within each thickness group. This seemingly backwards correlation can be explained by the strengthening of rivets as they form. Rivets which happen to form very quickly initially will be more formed in the end, but they also strengthen sooner and are thus observed to form more slowly in later hits. Using this negative correlation with total height change, late height change per hit was adjusted for initial rivet strengthening. The adjusted height change per hit varied 43% steadily with the 49% variation in coupon thickness, while bar momentum varied 18% with coupon thickness. The adjusted height change per hit correlated positively with bar

momentum with a 95% confidence range for the correlation coefficient of 0.58 to 0.82. A significant effect of free edge distance appeared but in a direction that contradicts the direction hypothesized for it. Besides the strong variation in bar momentum caused by thickness, no variation in bar momentum was observed to create a corresponding variation in adjusted formation rate. This either means that coupon thickness affects formation rate through a mechanism other than momentum absorption or that the true variation in bar momentum within each thickness was smaller than measurement error.

7.4 Extensions

Further experiments on this subject would benefit from measuring the motion of the coupon. The ability to subtract the coupon's position from the bucking bar's position would provide accurate rivet tail height measurements for every hit, including initial hits. This information could provide insight into why rivets on the middle thickness of coupon seem to have formed more in the first three hits than rivets on the other two coupons. Knowledge of the coupon's motion could also reveal how the motion changes with rivets near edges. Simulating the motion of the panel would allow the prediction of factor levels are likely to produce a significant result. Due to flexibility of the coupons used in this experiment, it is possible that the rivets were not tested close enough to an edge to observe the edge's predicted effects. Seemingly random effects with position did appear, but these may be a product of the resonance of the coupon before each strike interfering with measurements.

Additional factors which would be informative to vary are the bucking bar mass, the number of plies in the coupon (a single, solid ply or two plies joined together), and the presence of previously installed rivets, particularly on double-ply coupons. Finally, an experiment

comparing a standard coupon with a mock specimen of an aircraft panel would more concretely address the question of whether riveting on a coupon accurately represents riveting on an aircraft.

7.5 Recommendations

Particularly when a light bucking bar is used, percussive riveting varies substantially with the thickness of the workpiece. Tools which install rivets quickly in test can be expected to take longer to install rivets in workpieces which are thicker than the coupon used to test them. On the other hand, a bucking bar used on a workpiece which is thinner than the coupon on which it was tested is likely to receive more momentum from the rivet, transmitting more harmful vibration to the operator than predicted in test.

Bibliography

[1] Jonathan Ahn, "Methods for Evaluating the Performance and Human Stress-Factors of Percussive Riveting." Master of Science thesis, University of Washington, Seattle, WA, 2017.

[2] Thomas W. McDowell, Christopher Warren, Xueyan Xu, Daniel Welcome, Ren Dong, "Laboratory and Workplace Assessments of Rivet Bucking Bar Vibration Emissions." The Annals of Occupational Hygiene, vol. 59 (3), pp. 382-397. April 2015. [Online]. Available: Oxford Academic, academic.oup.com [Accessed June 3, 2018].

[3] John G. Cherng, Mahmut Eksioglu, Kemal Kizilaslan. "Vibration reduction of pneumatic percussive rivet tools: Mechanical and ergonomic re-design approaches." Applied Ergonomics, vol. 40 (2), pp. 256-266, March 2009. [Online] Available: ScienceDirect, www.sciencedirect.com [Accessed June 3, 2018].

[4] Krister Engström, Rolf Dandanell, "Exposure conditions and Raynaud's phenomenon among riveters in aircraft industry," Scandinavian Journal of Work, Environment and Health, vol. 12 (4), pp. 293-295. [Online serial] Available: http://www.sjweh.fi/show_abstract.php?abstract_id=2138. [Accessed June 3, 2018].

[5] Feng-Feng Xi, Lin Yu, Xiao-Wei Tu. "Framework on robotic percussive riveting for aircraft assembly automation." Advances in Manufacturing, Vol. 1 (2), pp. 112-122, June 2013. [Online]. Available: Springer, link.springer.com [Accessed June 3, 2018].

[6] Marc Thomas, Frederic Laville, Yves Beauchamp, and Ferdinand Simard. "An Experimental Design for Reducing Riveting Noise." In Proc. 22nd International Conference on Computers and Industrial Engineering, December 1997, pp 435-438. [Online] Available: www.researchgate.net, [Accessed June 3, 2018].

[7] Johan Hedekäll. "Re: Fwd: RRH information." Personal E-mail (Aug 25, 2015).

[8] University of Colorado Boulder, "Chapter 17: Modelling for Plate Vibrations.", www.colorado.edu, Mar. 16, 2004. [Online]. Available: https://www.colorado.edu/engineering/CAS/courses.d/IADYN.d/ASEN5022.slide.17.pdf, [Accessed Feb. 6, 2018]

[9] Bhalchandra Ballal. "Vibrations of Rectangular Plates," M.S. thesis, Rice University, Houston, TX, July 1966. [Online]. Available: scholarship.rice.edu [Accessed June 3, 2018].

[10] Fadil Santosa, Yih-Hsing Pao, "Transient Axially Asymmetric Response of an Elastic Plate." Wave Motion, vol. 11 (3), 271-295, June 1989. [Online] Available: ScienceDirect, www.sciencedirect.com [Accessed June 3, 2018].

Appendix A

Coupon machining

The rivets' holes were counterbored on the rivet-tail side of the coupon. This hole feature was designed to ensure the rivet tails would protrude a consistent height of 0.250" across coupons of all thicknesses. The rivets tail heights before formation averaged 249.5 thou, but because of imprecision in the machining they varied with a standard deviation of 1.4 thou. If variation in the initial tail heights are a factor in any outcome, and that variation happens to correlate with any factor, then the effect of such a factor on such an outcome may be an artifice of the machining error.

The following analysis is presented to demonstrate firstly that the machining error in the counterbore depths was not confounded with the experiment factors. Secondly, it shows that machining error did not significantly affect the experiment outcomes. This permits the conclusion that machining error did not interfere with the experiment results significantly enough to reject the experiment results.

A.1 Initial tail height vs. experiment factors

A model fit to the unformed tail heights in terms of the experiment factors of coupon thickness, distance from fixed edge, and distance from free edge found no term to have a significance level less than 0.095. The ANOVA results are shown in Table A.1.

Table A.1: Initial tail heights, thou, ANOVA with all terms

Source	d.f.	Prob>F
Thickness	2	0.721
Free edge	2	0.112
Fixed edge	3	0.483
Thickness*Free edge	4	0.130
Thickness*Fixed edge	6	0.0951
Free edge*Fixed edge	6	0.352
Error	45	
Total	68	

Most importantly, the means of initial heights for the three coupon thicknesses were too close together (within 4 tenths of a thou) to be significantly different. Within each coupon thickness, however, a nearly significant variation with free edge distance exists. Figure A.1 shows this variation is particularly in the third row of the 190 thou thick coupon and the second row of the 313 thou thick coupon.

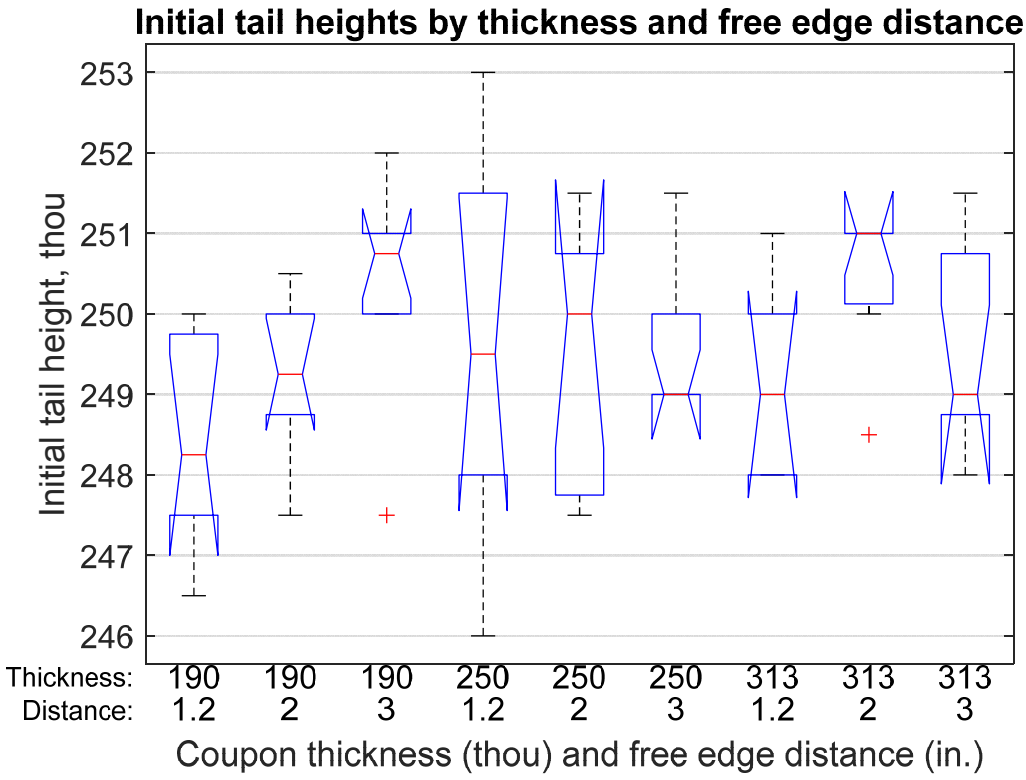

Figure A.1: Initial tail heights by thickness and free edge distance

Note that the boxes in Figure A.1 for the two highest groups are drawn excluding one each of the eight points from each group as outliers. The other analyses here include these points, drawing the mean of these groups toward the overall mean and reducing the effect of initial rivet height on the results by row.

We can conclude that coupon thickness is not confounded with initial rivet height as a factor in these rivets. Position on the coupon may be confounded with initial rivet height, but the correlation between those two factors is not strong.

A.2 Initial rivet tail vs. experiment outcomes

We now turn to the effect of initial tail height on the experiment outcomes. The effects of coupon thickness on these outcomes are too strong to be the product of correlation of the initial rivet height to the coupon thickness, as no correlation between initial height and coupon thickness was found. Therefore, we can subtract the effect of coupon thickness from the experiment outcomes to better assess the strength of other effects. We will not be also subtracting the effect of initial tail height by doing so. The following four figures show the correlation of initial tail height with each experiment outcome – tail height change, bar momentum, height change per hit, and adjusted height change per hit.

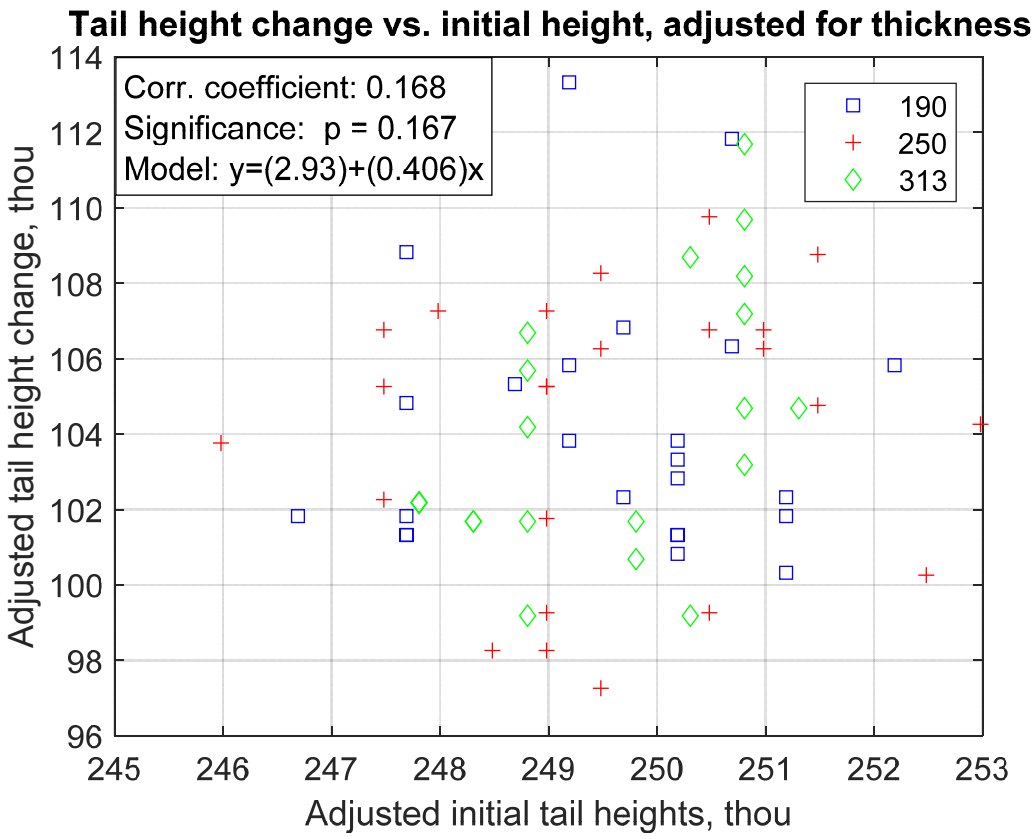

Figure A.2: Tail height change vs. initial height, adjusted for thickness

Figure A.3 shows that a small positive correlation between initial tail height and final height change may exist. If so, the final rivet height changes approximately 0.4 thou per thou of initial tail height.

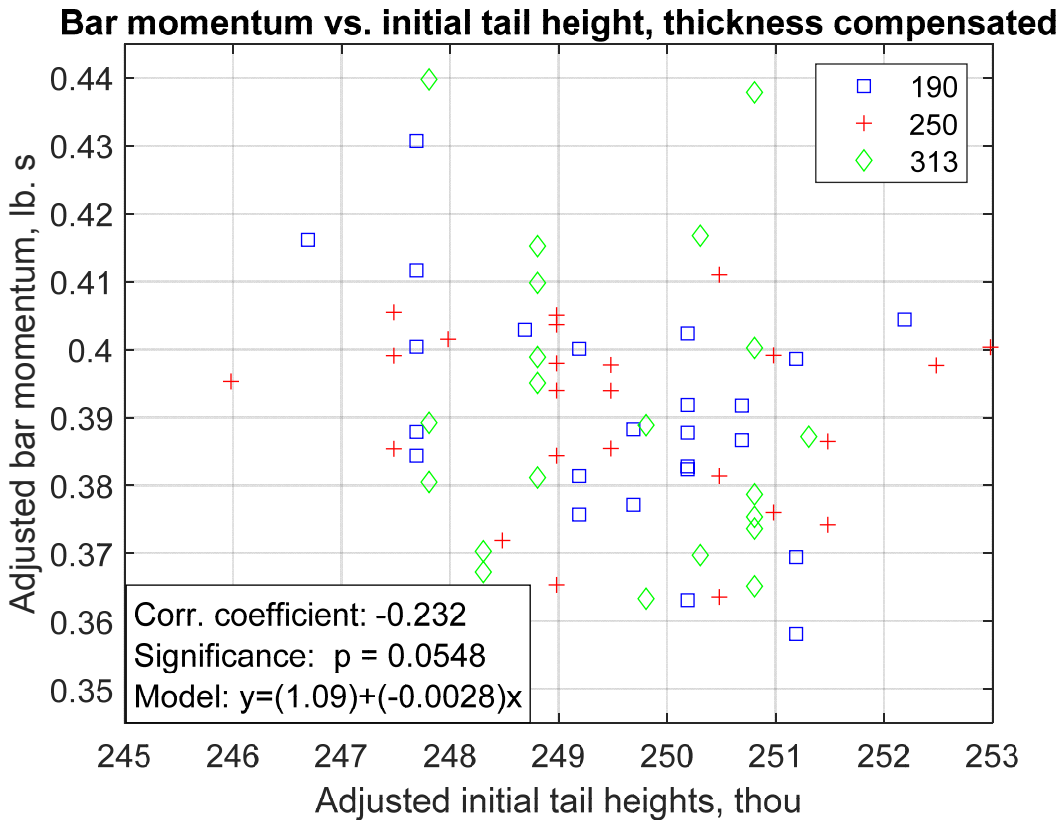

Figure A.3: Bar momentum vs. initial tail height, thickness compensated

Figure A.3 shows a small negative correlation between the bar momentum and the initial tail height likely does exist. This correlation is on the threshold of statistical significance, indicating that the machining error was probably a small source of variation in the bar momentum.

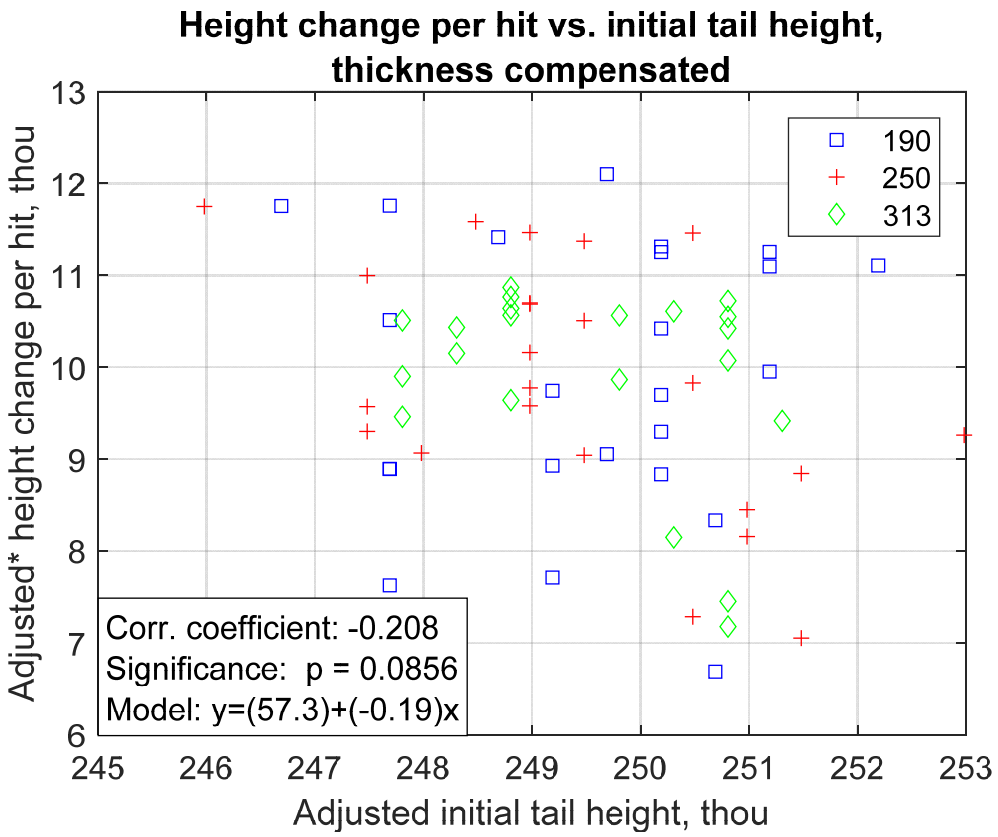

Figure A.4: Height change per hit vs. initial tail height, thickness compensated.

*Height change per hit adjusted for thickness, not total height change

Figure A.4 shows that a small negative correlation may exist between height change per hit and initial tail height.

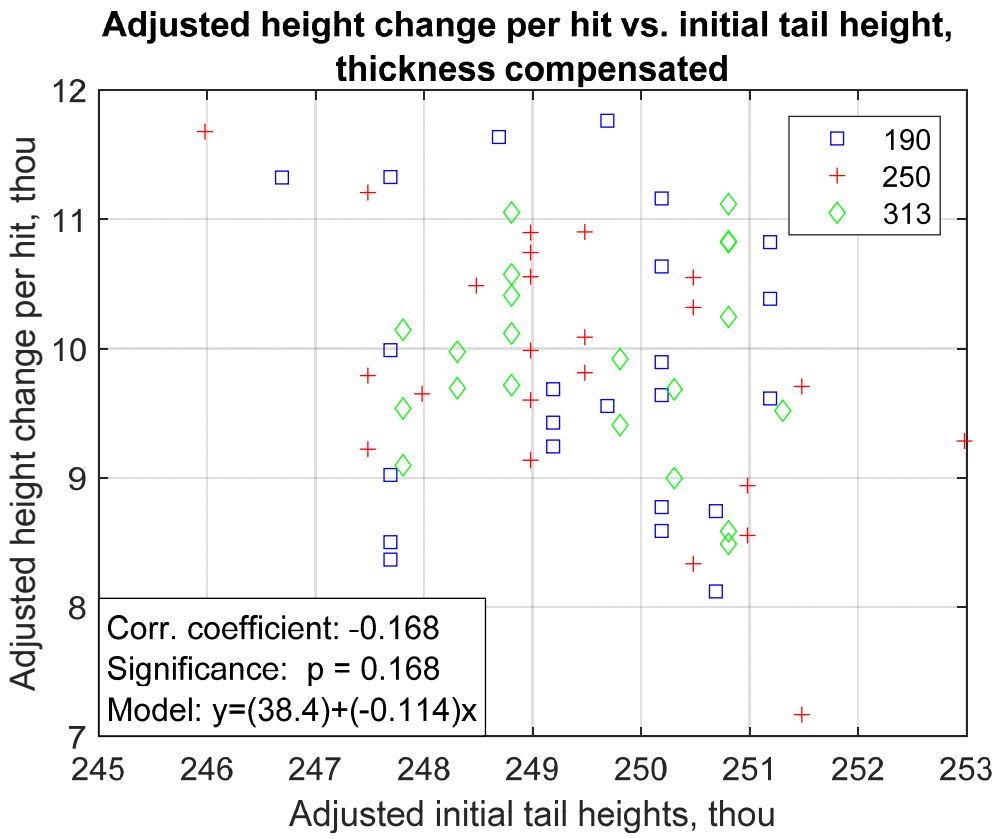

Figure A.5: Adjusted* height change per hit vs. initial tail height, thickness compensated

*Note that the height change per hit is adjusted both for total height change and for coupon thickness, while the initial tail height is only adjusted for coupon thickness.

Figure A.5 shows that some of the correlation between height change per hit and initial tail height is probably lost when adjusting height change for final rivet height change.

In conclusion, counterboring successfully decoupled initial rivet tail height with coupon thickness. Initial rivet tail height probably varied enough to affect the experiment outcomes, but it did not correlate strongly with any experiment factors. Therefore, the effects of initial tail height were not likely to be confounded with the effects of rivet position and certainly not and not confounded with the effects of coupon thickness.

Appendix B

Random ordering of rivet installations

Table B.2 and Table B.3 show the randomized order in which rivets were installed in the coupon halves and positions on each half, respectively.

Table B.2: Order in which halves of coupons were filled

		Coupon thickness (thou)		
		190	250	313
Side	A	2	3	1
	B	5	4	6

Table B.3: Order in which rivets were installed in each half of each coupon

		Fixed edge distance (in.)			
		1.9	3.5	5.1	6.7
Free edge distance (in.)	2	4	1	11	10
	3	9	6	3	8
	1.2	7	12	5	2

Appendix C

ANOVA analysis, interaction models and significant term models

This section supports the selection terms to include in the linear models presented in sections 5 and 6. First an ANOVA is presented with all main effects and two-factor interactions. A follow-up ANOVA is presented with only the terms the previous ANOVA identified as statistically significant ($p \leq 0.05$). Where no significant interaction terms are present, a main effects plot is then included. Where only two factors are significant, or when two factors have a significant interaction, a box plot is included showing each combination of those two factors as its own group.

Confidence levels are calculated based on the variance of the data itself and assumptions about the data's distribution – no "a priori" estimates of the distributions of the measurement error were incorporated into the confidence estimates. This is probably why the confidence levels produced by the ANOVA below are often higher than the measurement methods justify for apparently random trends. More rigorous statistical analysis is necessary to obtain confidence levels which accurately reflect the uncertainty of the measurement methods. Given the depth of the analysis here, we can still distinguish between the significant effects of coupon thickness and the generally marginal effects of rivet position.

C.1 Rivet height changes

Table C.4: Rivet tail height change ANOVA with interaction model

Source	d.f.	Prob>F
Thickness	2	4.66E-13
Free edge	2	0.0437
Fixed edge	3	0.149
Thickness*Free edge	4	0.155
Thickness*Fixed edge	6	0.564
Free edge*Fixed edge	6	0.238
Error	45	
Total	68	

Table C.5: Rivet tail height change ANOVA with statistically significant terms in model

Source	d.f.	Prob>F
Thickness	2	6.50E-14
Free edge	2	0.037
Error	64	
Total	68	

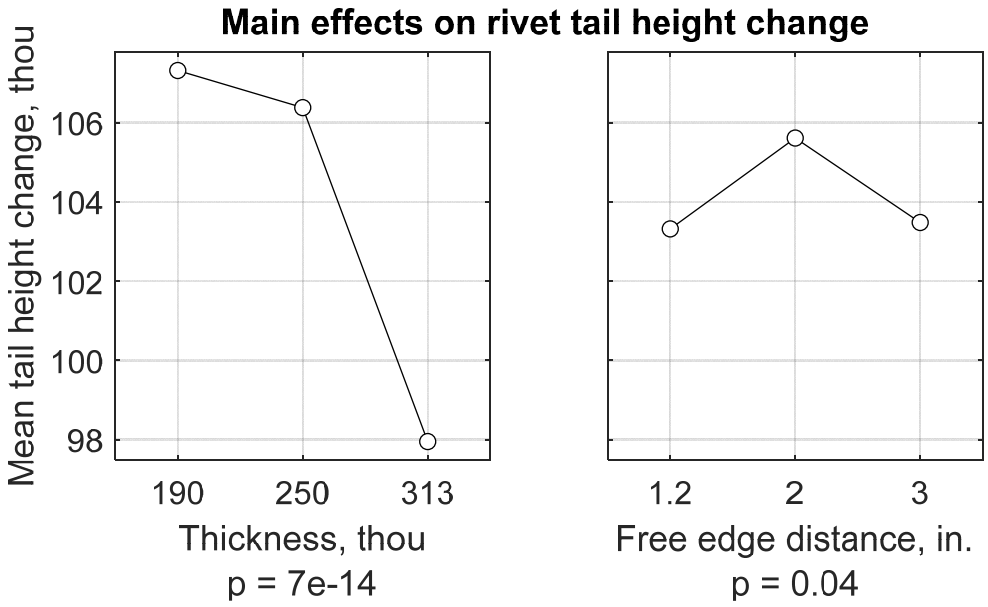

Figure C.6: Main effects on rivet tail height change, significant terms

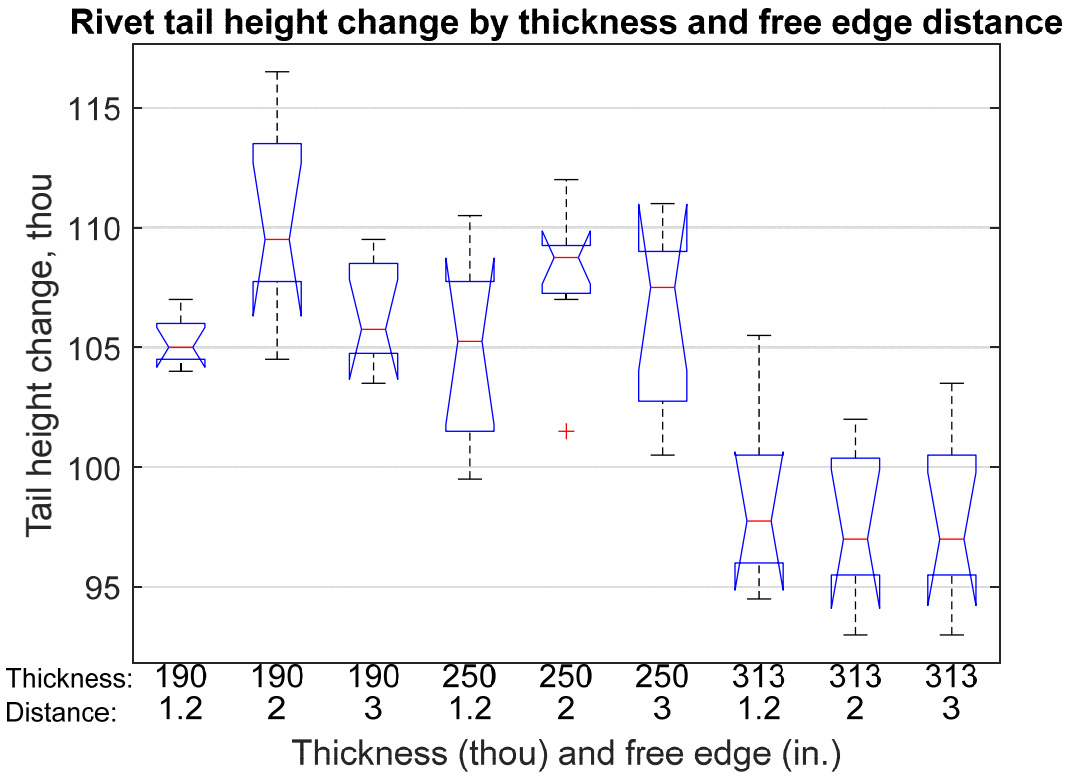

Figure C.7: Rivet tail height change by thickness and free edge distance

C.2 Bar momentum

Bar momentum estimated from bar position measurements, using mean of hits 4-6.

Table C.6: Bar momentum ANOVA, with interaction model

Source	d.f.	Prob>F
Thickness	2	3.94E-20
Free edge	2	4.01E-05
Fixed edge	3	0.131
Thickness*Free edge	4	0.000704
Thickness*Fixed edge	6	0.0355
Free edge*Fixed edge	6	0.175
Error	45	
Total	68	

Table C.7: Bar momentum ANOVA, significant terms

Source	d.f.	Prob>F
Thickness	2	2.15E-21
Free edge	2	0.000405
Thickness*Free edge	4	0.0069
Error	60	
Total	68	

* An interaction between thickness and fixed edge distance (significance level 0.0355) was omitted because the main effect fixed edge of fixed edge distance was insignificant (significance level 0.131)

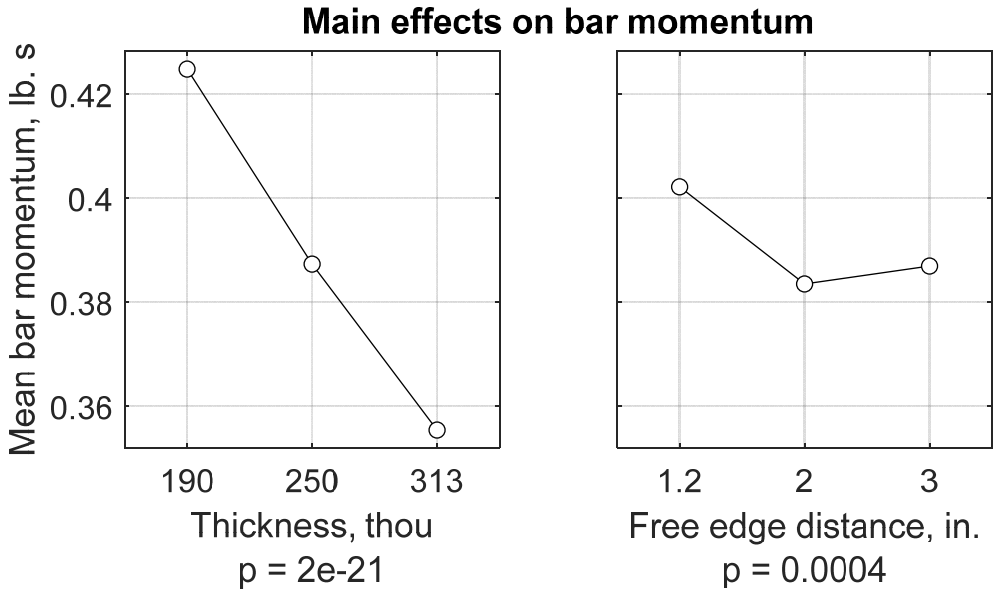

Figure C.8: Main effects on bar momentum, significant terms

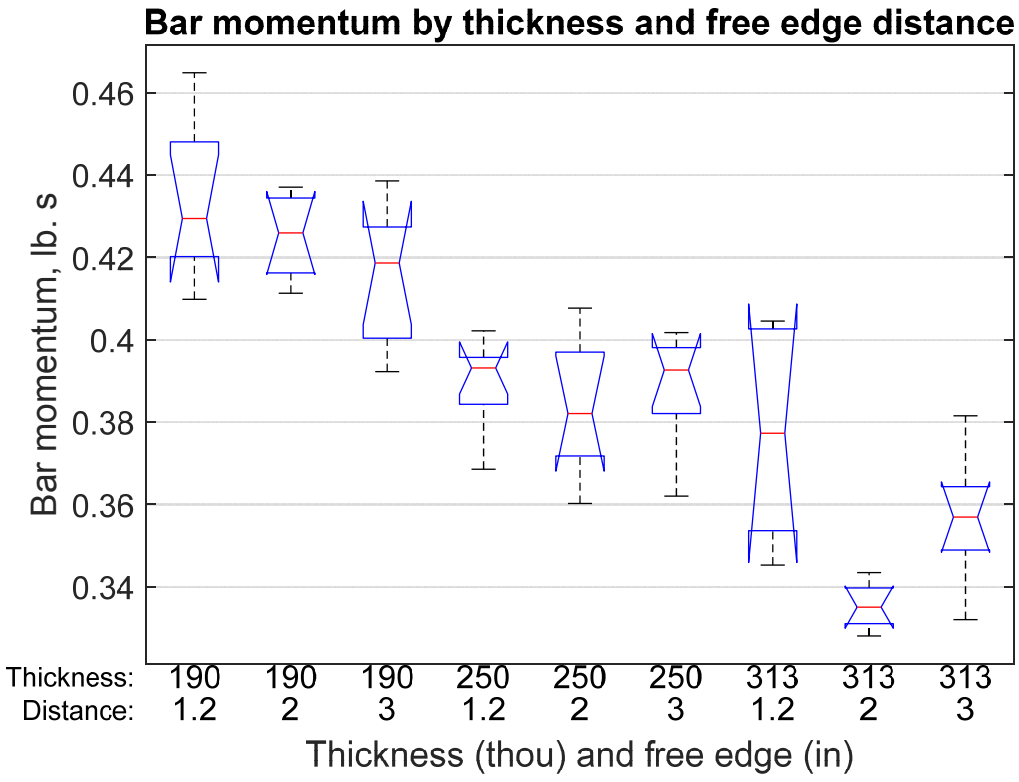

Figure C.9: Bar momentum by thickness and free edge distance

C.3 Formation per hit

Table C.8: Height change per hit ANOVA, with interaction model

Source	d.f.	Prob>F
Thickness	2	2.02E-09
Free edge	2	0.0397
Fixed edge	3	0.023
Thickness*Free edge	4	0.0838
Thickness*Fixed edge	6	0.458
Free edge*Fixed edge	6	0.524
Error	45	
Total	68	

Table C.9: Height change per hit, thou, ANOVA with significant terms

Source	d.f.	Prob>F
Thickness	2	6.07E-10
Free edge	2	0.0329
Fixed edge	3	0.0291
Error	61	
Total	68	

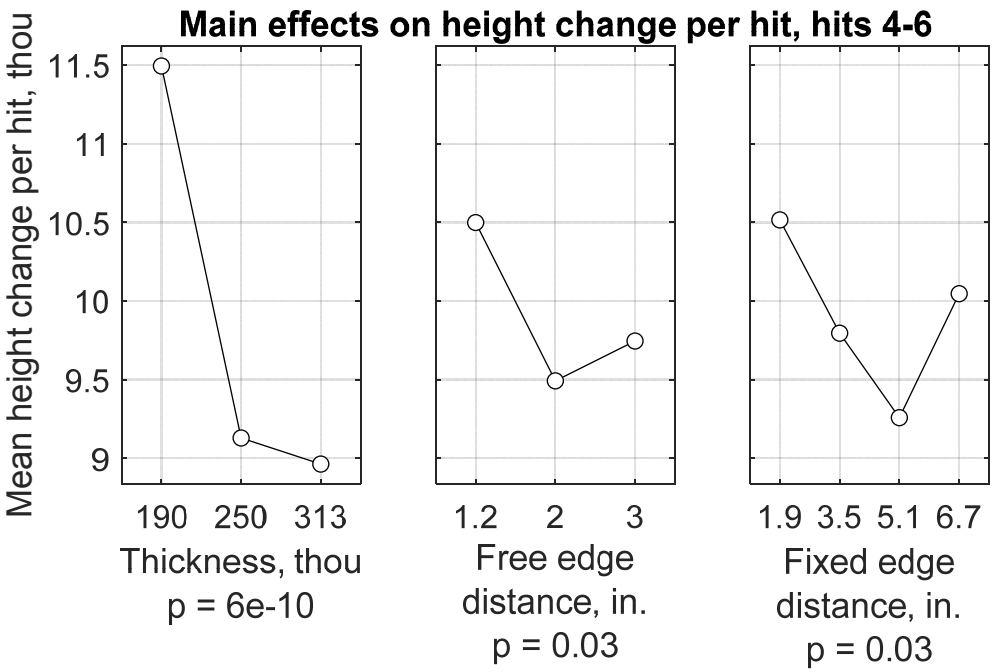

Figure C.10: Main effects on height change per hit, hits 4-6

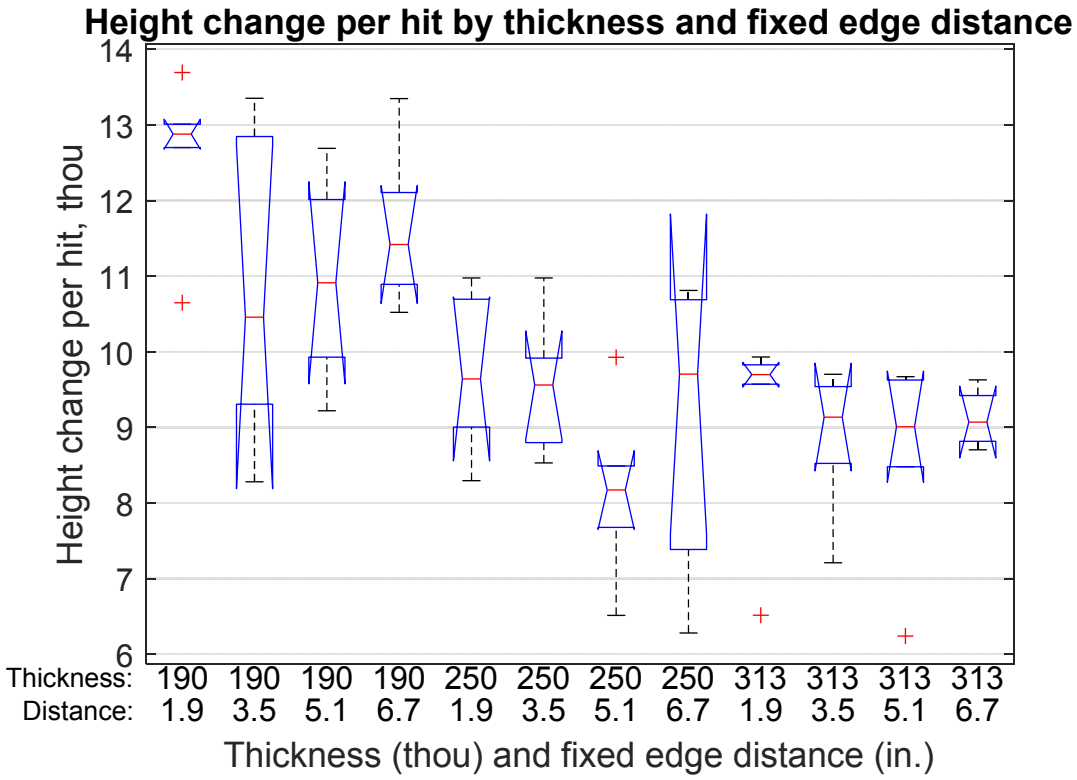

Figure C.11: Height change per hit by thickness and fixed edge distance

A model including only one interaction term – interaction between coupon thickness and distance from free edge – indicates that free edge distance term and the thickness-free edge interaction term are on the edge of statistical significance. Table C.10 lists these ANOVA results, and Figure C.12 compares the height change per hit for nine groups at each combination of coupon thickness and free edge distance.

Table C.10: Height change per hit ANOVA, significant or nearly significant terms in model

Source	d.f.	Prob>F
Thickness	2	1.96E-10
Free edge	2	0.0494
Fixed edge	3	0.0194
Thickness*Free edge	4	0.0527
Error	57	
Total	68	

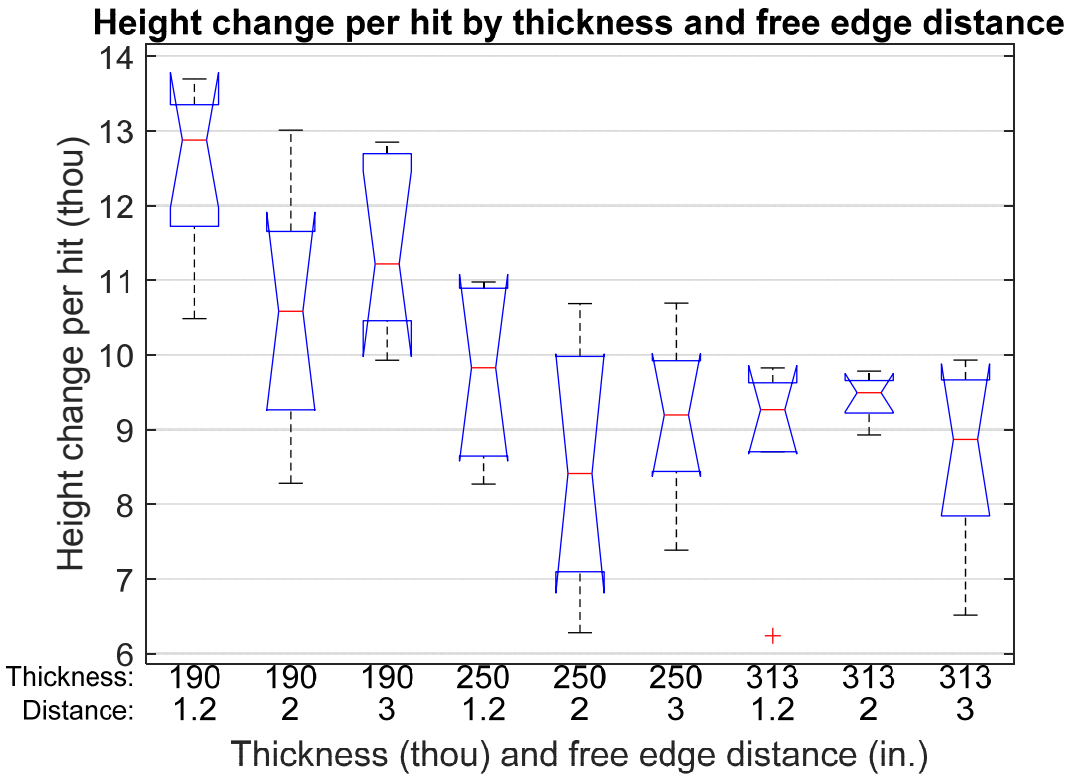

Figure C.12: Height change per hit by thickness and free edge distance

C.4 Adjusted formation per hit

Table C.11: Adjusted formation per hit, thou, ANOVA with all terms

Source	d.f.	Prob>F
Thickness	2	2.35E-20
Free edge	2	0.0813
Fixed edge	3	0.000239
Thickness*Free edge	4	0.211
Thickness*Fixed edge	6	0.251
Free edge*Fixed edge	6	0.618
Error	45	
Total	68	

Table C.12: Adjusted formation per hit, thou, ANOVA with significant terms

Source	d.f.	Prob>F
Thickness	2	1.09E-23
Fixed edge	3	0.000252
Error	63	
Total	68	

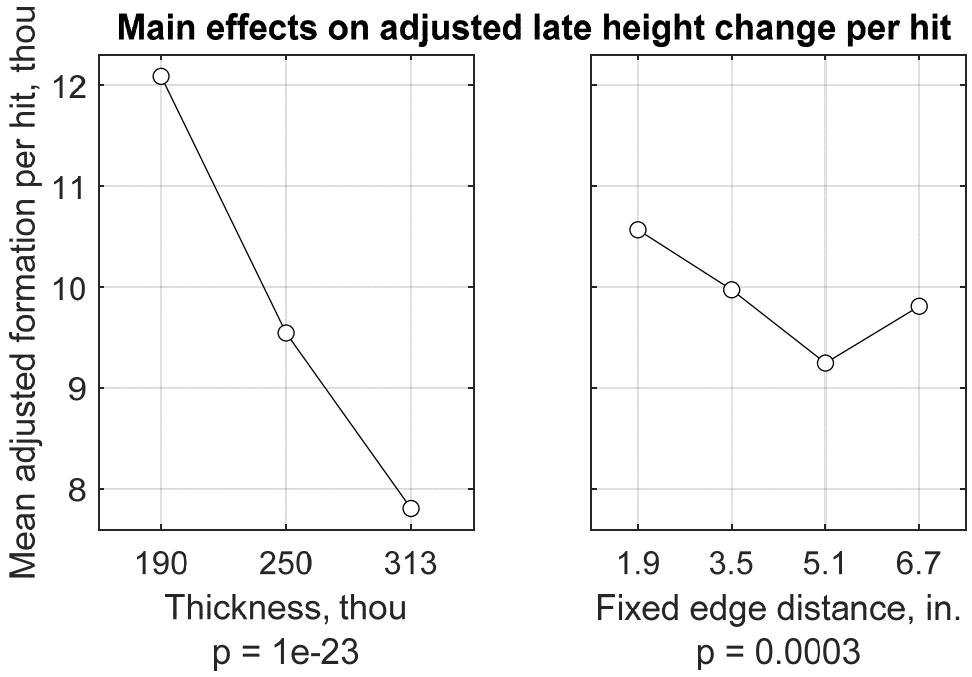

Figure C.13: Main effects on adjusted late height change per hit

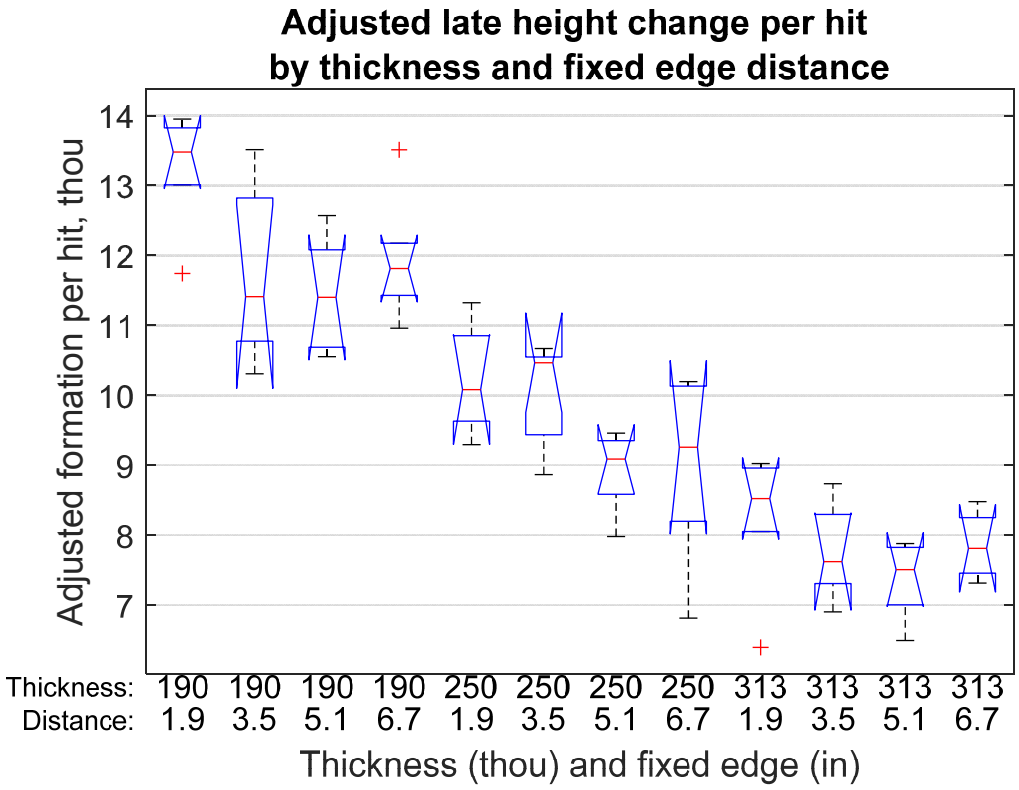

Figure C.14: Adjusted height change per hit, by thickness and fixed edge distance